Identification of Novel Low Molecular Weight CXCR4 Antagonists by Structural Tuning of Cyclic Tetrapeptide Scaffolds

Hirokazu Tamamura,*[,⊥,#] Takanobu Araki,[⊥] Satoshi Ueda,[⊥] Zixuan Wang,[§] Shinya Oishi,[⊥] Ai Esaka,[⊥] John O. Trent,[∥] Hideki Nakashima,[†] Naoki Yamamoto,[‡] Stephen C. Peiper,[§] Akira Otaka,[⊥] and Nobutaka Fujii*[,⊥]

Graduate School of Pharmaceutical Sciences, Kyoto University, Sakyo-ku, Kyoto 606-8501, Japan; Institute of Biomaterials and Bioengineering, Tokyo Medical and Dental University, Chiyoda-ku Tokyo 101-0062, Japan; Medical College of Georgia, Augusta, Georgia 30912; James Graham Brown Cancer Center, University of Louisville, Louisville, Kentucky 40202; St. Marianna University, School of Medicine, Miyamae-ku, Kawasaki 216-8511, Japan; and Tokyo Medical and Dental University, School of Medicine, Bunkyo-ku, Tokyo 113-8519, Japan

Received January 5, 2005

A highly potent CXCR4 antagonist, compound **2**, was previously found by using two orthogonal cyclic pentapeptide libraries involving conformation-based and sequence-based libraries based on the pharmacophore of a 14-mer peptidic antagonist, **1**. Herein, cyclic tetrapeptides derived from replacements of the dipeptide unit (Nal-Gly) with a γ-amino acid and pseudopeptides cyclized by disulfide and olefin bridges were synthesized to find novel scaffold structures different from that of cyclic pentapeptides. These compounds contain a reduced number of peptide bonds compared to compound **2**. Furthermore, several analogues with chemical modification of the side chain of Arg^4 in **2** were also prepared. From these, several new leads possessing high to moderate CXCR4-antagonistic activity were characterized.

Introduction

The chemokine receptor, CXCR4, is a seven transmembrane (7TM) GPCR that transduces signals of its endogenous ligand, stromal cell-derived factor-1 (SDF-1).[1−4] The SDF-1/CXCR4 system plays an important role in the migration of progenitors during embryologic development of the cardiovascular, hemopoietic, and central nervous systems. Recently, this system has been shown to be involved in several diseases, including HIV infection,[5] cancer metastasis/progression,[6−20] and rheumatoid arthritis (RA).[21] CXCR4 was initially identified as a coreceptor that is utilized in T cell line-tropic (X4-) HIV-1 entry.[5] Müller et al. reported that CXCR4 and another chemokine receptor, CCR7, are highly expressed in human breast cancer cells, while SDF-1 and a CCR7 ligand, CCL21, are highly expressed in lymph nodes, bone marrow, lung, and liver, which represent the primary metastatic destinations of breast cancer, suggesting that the SDF-1/CXCR4 system might determine the metastatic destination of tumor cells.[6] Recently, this system has been recognized to be involved in the metastasis of several types of cancers, such as pancreatic cancer,[7,8] melanoma,[6,9] prostate cancer,[10] kidney cancer,[11] neuroblastoma,[12] non-Hodgkin's lymphoma,[13] lung cancer,[14] ovarian cancer,[15,16] multiple myeloma,[17] chronic lymphocytic leukemia,[18] acute lymphoblastic leukemia,[19] and malignant brain tumor.[20] Nanki et al. reported that the memory T cells highly express CXCR4 and the SDF-1 concentration is extremely high in the synovium of RA patients, and that

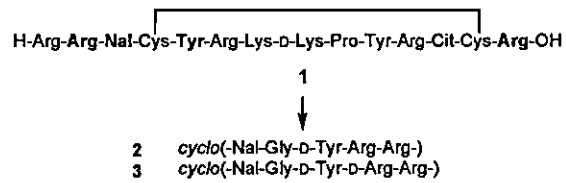

Figure 1. Reduction of the molecular size of a peptide **1** to cyclic pentapeptides **2** and **3**. Bold residues are the indispensable residues of **1** for the expression of strong CXCR4-antagonistic activity.

SDF-1 stimulates migration of the memory T cells and inhibits T cell apoptosis, indicating that the SDF−CXCR4 interaction plays a critical role in T cell accumulation in the RA synovium.[21] Thus, CXCR4 is thought to be an important therapeutic target for these diseases. Compound **1** and its analogues, 14-mer peptides, were previously found to be specific CXCR4 antagonists that were characterized as HIV-entry inhibitors,[22] anticancer-metastatic agents[8,23] and anti-RA agents.[24] Arg^2, L-3-(2-naphthyl)alanine (Nal)[3], Tyr^5, and Arg^{14} were proven to constitute the critical pharmacophores of **1** (Figure 1).[25] The efficient utilization of two orthogonal cyclic pentapeptide libraries consisting of conformation-based and sequence-based libraries involving the critical residues of **1** led to molecular-size reduction of **1** and discovery of cyclic pentapeptides, **2** and **3**, which have strong CXCR4-antagonistic activity, comparable to that of **1**.[26] In this paper, we describe the fine-tuning of ring structures based on cyclic pentapeptide templates,[27−34] and chemical modifications of side chains for an increase in potency and a reduction of the peptide characteristics of **2**.[35]

Chemistry

γ-Amino Acid-Containing Cyclic Tetrapeptides (11a−d). Requisite N^{γ}-Fmoc-γ-amino acids, (2*E*,4*S*)-N^{γ}-

* Corresponding authors. Tel: +81 75 753 4551, Fax: +81 75 753 4570, e-mail: tamamura@pharm.kyoto-u.ac.jp and nfujii@pharm.kyoto-u.ac.jp.
[⊥] Kyoto University.
[#] Institute of Biomaterials and Bioengineering.
[§] Medical College of Georgia.
[∥] University of Louisville.
[†] St. Marianna University.
[‡] School of Medicine.

10.1021/jm050009h CCC: $30.25
Published on Web 04/13/2005

Scheme 1[a]

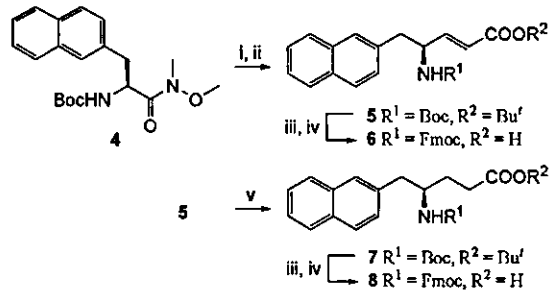

[a] Reagents: (i) DIBAL-H; (ii) $(EtO)_2P(O)CH_2CO_2Bu^t$,LiCl, DIPEA; (iii) 95% aqueous TFA; (iv) Fmoc-OSu, Et_3N; (v) H_2, Pd/C.

Scheme 2[a]

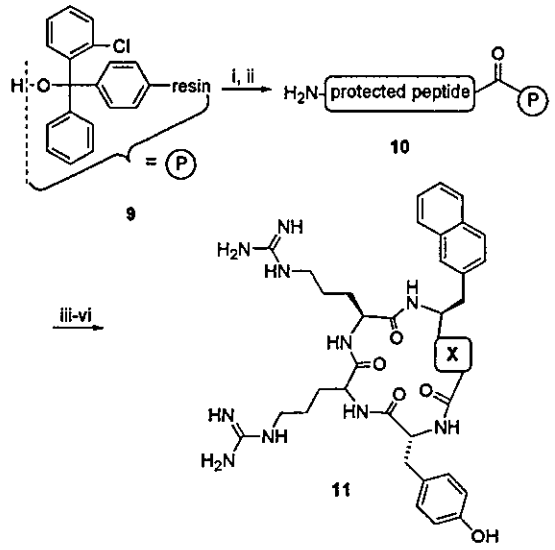

Compd.	Sequence (*cyclo*)	X
11a	(-γ-Nal[1]-D-Tyr[2]-D-Arg[3]-Arg[4]-)	$-CH_2-CH_2-$
11b	(-γ-Nal[1]-D-Tyr[2]-Arg[3]-Arg[4]-)	$-CH_2-CH_2-$
11c	(-γ-(*E*)-Nal[1]-D-Tyr[2]-D-Arg[3]-Arg[4]-)	-CH=CH-
11d	(-γ-(*E*)-Nal[1]-D-Tyr[2]-Arg[3]-Arg[4]-)	-CH=CH-

[a] Reagents: (i) **6** or **8**, DIPEA, DMF/CH_2Cl_2; (ii) Fmoc-based SPPS; (iii) AcOH/TFE/CH_2Cl_2; (iv) DPPA, $NaHCO_3$; (v) basic alumina column; (vi) 95% aqueous TFA.

Fmoc-4-amino-5-naphthalen-2-yl-pent-2-enoic acid (γ-(*E*)-Nal) **6** and (4*R*)-*N*γ-Fmoc-4-amino-5-naphthalen-2-yl-pentanoic acid (γ-Nal) **8**, were synthesized according to Scheme 1. Boc-Nal-NMe(OMe) **4** was treated with DIBAL followed by modified Horner–Wadsworth–Emmons olefination to yield Boc-γ-(*E*)-Nal-OBu^t **5**. *N*$^\alpha$-Fmoc-protection after the cleavage of the *N*$^\alpha$-Boc and Bu^t groups of **5** with TFA afforded a desired compound, Fmoc-γ-(*E*)-Nal-OH **6**. Hydrogenation of **5** obtained a reduced compound, **7**, which was similarly converted to another desired compound, Fmoc-γ-Nal-OH **8**. The protected peptide resin **10** was constructed by general Fmoc-based solid-phase synthesis on a (2-chloro)trityl resin **9**, in which the above γ-amino acid, **6** or **8**, was introduced as a C-terminal residue by DIPEA in DMF/CH_2Cl_2 (Scheme 2). Cleavage of the liner peptide from the resin with AcOH/TFE/CH_2Cl_2 (1:1:3 (v/v)) followed by cyclization with diphenylphosphoryl azide (DPPA) and $NaHCO_3$, subsequent deprotection with TFA and HPLC purification gave the desired cyclic peptide **11**.[26]

Scheme 3[a]

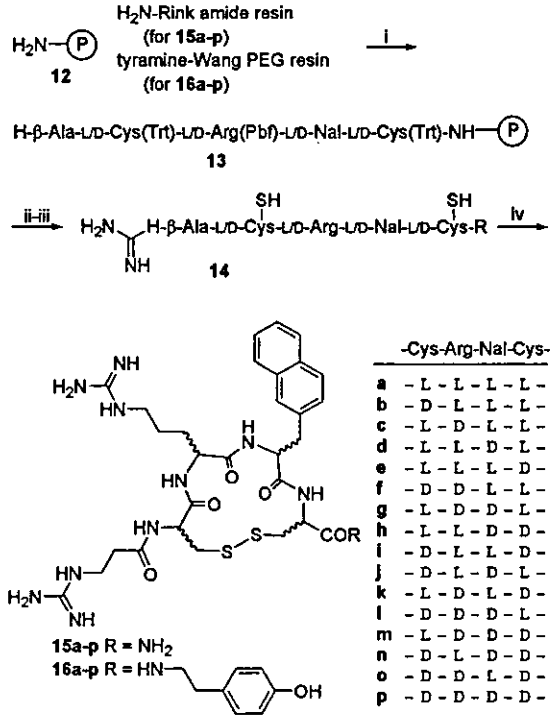

[a] Reagents: (i) Fmoc-based SPPS; (ii) 1*H*-pyrazole-1-carboxamidine hydrochloride, DIPEA; (iii) EDT/H_2O/TFA; (iv) aqueous $AcONH_4$ pH 8.

Disulfide-Bridged Cyclic Peptides (15a–p and 16a–p). The protected peptide resin was constructed by general Fmoc-based solid-phase synthesis on an NH_2-Rink amide resin (for **15a–p**) or a tyramine-Wang PEG resin (for **16a–p**) **12** (Scheme 3). Fmoc-β-Ala-OH was condensed to the N-terminus of the protected resin as the final residue. After deprotection of the Fmoc group, N-guanylation of the resulting free β-amino group with 1*H*-pyrazole-1-carboxamidine hydrochloride and DIPEA, followed by cleavage from the resin and removal of the 2,2,4,6,7-pentamethyldihydrobenzofuran-5-sulfonyl (Pbf) and Trt groups with EDT/H_2O/TFA, gave the crude reduced peptide (2SH-peptide) **14**. Subsequent air-oxidation of the crude 2SH-peptide **14** and HPLC purification yielded the desired disulfide peptide **15** or **16**.

Disulfide-Bridged Cyclic Peptides (15q and 16q). The protected peptide resin was constructed on an Fmoc-NH-Rink amide resin (for **15q**) or an Fmoc-tyramine-Wang PEG resin (for **16q**) in the same manner as in the synthesis of **15e** or **16e** (Table 1). Reductive amination of the N-terminal amino group of the protected resin with *N*-Fmoc-3-aminopropanal and $NaBH(OAc)_3$,[36] followed by removal of the Fmoc group and the subsequent N-guanylation of the resulting free amino group in the same manner as in the synthesis of **15e** or **16e**, obtained the protected pseudo-peptide resin. Cleavage from the resin and removal of the Pbf and Trt groups, the subsequent air-oxidation, and HPLC purification were performed in the same manner as in the

Table 1. Inhibitory Activity of Disulfide/Olefin-Bridged Cyclic Peptides against SDF-1 Binding to CXCR4

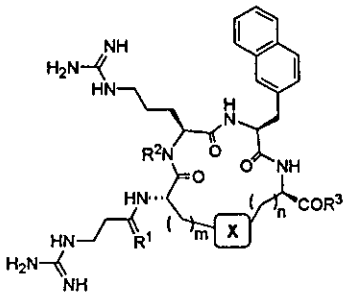

compd	m	n	X	R^1	R^2	R^3	$IC_{50} \pm SD$ (μM)[a]
15e	1	1	S–S	O	H	NH_2	0.69 ± 0.40
16e	1	1	S–S	O	H	tyramine	0.53 ± 0.28
15q	1	1	S–S	H_2	H	NH_2	ca. 1
16q	1	1	S–S	H_2	H	tyramine	ca. 1
15r	1	1	S–S	O	Me	NH_2	>10
16r	1	1	S–S	O	Me	tyramine	>10
20a	1	1	(*E*)-CH=CH	O	H	NH_2	1–10
20b	1	2	(*E*)-CH=CH	O	H	NH_2	1–10
20c	2	2	(*E*)-CH=CH	O	H	NH_2	1–10
20d	1	1	(*E*)-CH=CH	O	H	tyramine	1–10
2							0.0043 ± 0.0012
3							0.0084 ± 0.0038

[a] IC_{50} values are based on the inhibition of [^{125}I]-SDF-1 binding to CXCR4 transfectants of CHO cells. All data with standard deviation (SD) are the mean values for at least three independent experiments.

synthesis of **15e** or **16e** to yield the desired pseudopeptide, **15q** or **16q**.

Disulfide-bridged Cyclic Peptides (15r and 16r). The protected peptide resin was constructed on an Fmoc-NH-Rink amide resin (for **15r**) or an Fmoc-tyramine-Wang PEG resin (for **16r**) (Table 1). N^{α}-Methylation of the Arg(Pbf) residue in the protected resin was performed by the Fukuyama–Mitsunobu reaction.[37] N^{α}-*o*-Nitrobenzenesulfonyl (Ns) protection of H-Arg(Pbf)-Nal-D-Cys-NH-Rink amide (or -tyramine-Wang PEG) resin and the subsequent N^{α}-methylation with MeOH, Ph_3P, and diethyl azodicarboxylate (DEAD) were followed by removal of the N^{α}-Ns group with DBU and 2-mercaptoethanol. The next residue Fmoc-D-Tyr(Bu^t)-OH was condensed to the secondary N^{α}-amino group of the MeArg(Pbf) residue on the protected resin by using HATU, HOAt, and DIPEA. N-Guanylation, cleavage, deprotection, air-oxidation, and HPLC purification were subjected to yield the desired peptide, **15r** or **16r**.

Olefin-Bridged Cyclic Peptides (20a–d). The protected peptide resin was constructed on an NH_2-Rink amide resin (for **20a–c**) or an Fmoc-tyramine-Wang PEG resin (for **20d**) (Scheme 4) **12**. D-2-Allylglycine[38] (for **20a** or **20d**) or Fmoc-D-2-homoallylglycine[39,40] (for **20b** or **20c**) was used as the C-terminal residue, while Fmoc-L-2-allylglycine[41] (for **20a**, **20b**, or **20d**) or Fmoc-L-2-homoallylglycine[42] (for **20c**) was used as the N-terminal second residue. Fmoc-β-Ala-OH was condensed to the N-terminus of the protected resin as the final residue. The protected peptide resin **17** was subjected to ring-closing olefin metathesis with Grubbs catalyst second generation[43] to give the cyclized peptide resin **18**. After deprotection of the Fmoc group, N-guanylation of the resulting free β-amino group, followed by treatment with 1 M TMSBr-thioanisole/TFA and HPLC purification, gave the desired peptide **20**. The *E* geometry of the olefin units in **20a–d** was easily established from the coupling constants (J = 15.5, 15.6, 15.2, and 15.2 Hz, respectively) of the two olefinic protons by ^{1}H NMR analysis.

Scheme 4[a]

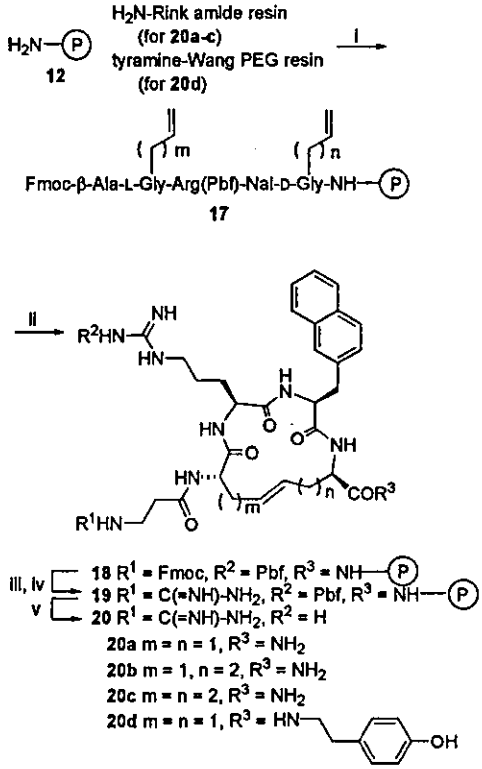

[a] Reagents: (i) Fmoc-based SPPS; (ii) Grubbs catalyst 2nd generation, (iii) piperdine; (iv) 1*H*-pyrazole-1-carboxamidine hydrochloride, DIPEA; (v) 1 M TMSBr-thioanisole/TFA.

Analogues with Substitution for Arg^4 (23a–p). Each peptide was synthesized in a general manner similar to that in the synthesis of **11a**. **23d** and **23f**: N^{α}-Methylation and coupling reaction to the N^{α}-methylated residue were performed in a manner similar to that in the synthesis of **15r**. **23j,k** and **23o,p**: After cyclization and deprotection, N-guanylation of the resulting free γ- or ϵ-amino group of the L-2,4-diaminobutyric acid (Dab)[4] or Lys[4] residue (for **23j** or **23k**, respectively) was performed with 1*H*-pyrazole-1-carboxamidine hydrochloride and DIPEA (Scheme 5). N-Guanylation of the resulting free γ-amino group of the *trans*- or *cis*-4-aminoproline residue[44] (for **23o** or **23p**, respectively) was similarly performed.

Biological Results and Discussion

γ-Amino Acid-Containing Cyclic Tetrapeptides. Cyclic pentapeptides, **2** and **3**, have a Gly residue as a spacer for cyclization. To reduce the ring size, the Nal-Gly sequences of **2** and **3** were replaced by a γ-Nal or γ-(*E*)-Nal unit (Scheme 2). Among these γ-amino acid-containing cyclic tetrapeptides (**11a–d**), only **11a** [substitution of γ-Nal for Nal-Gly of **3**] showed high CXCR4-antagonistic activity (IC_{50} = 54 nM) (Figure 2), although

Scheme 5[a]

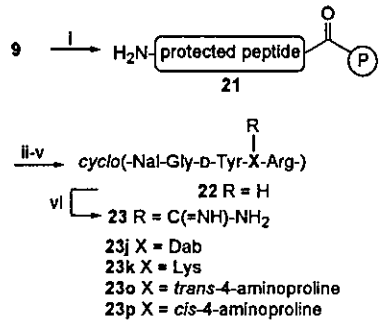

[a] Reagents: (i) Fmoc-based SPPS; (ii) AcOH/TFE/CH_2Cl_2 (1:1:3 (v/v)); (iii) DPPA, $NaHCO_3$; (iv) basic alumina column; (v) 95% aqueous TFA; (vi) 1*H*-pyrazole-1-carboxamidine hydrochloride, DIPEA.

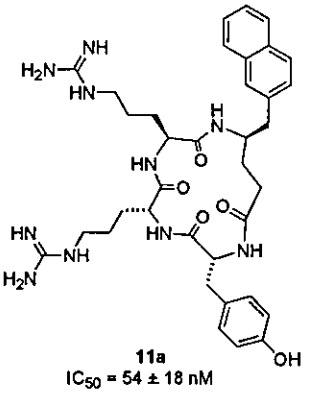

Figure 2. The structure of **11a**.

this activity is 6-fold lower than that of **3**. This result suggested that the Gly residue and the amide bond of the Nal-Gly sequence are not necessary for high activity. The reason for no significant activity of **11b** [substitution of γ-Nal for Nal-Gly of **2**] (IC_{50} > 1 μM) cannot be well explained, however, the difference of chirality of L/D-Arg^3 in **2** and **3** might cause a global conformational change of the ring. Both γ-(*E*)-Nal-substituted analogues, **11c** and **11d**, showed no significant activity (IC_{50} > 1 μM), suggesting that constraint of the γ-amino acid to the *E*-form might not be suitable.

Disulfide-Bridged Cyclic Peptides. To optimize the ring structures of compound **2**-derived compounds, the use of scaffold templates different from that of cyclic pentapeptides was investigated. Since the four requisite residues of **1** are disposed in close vicinity each other due to the disulfide bridge [Cys^4-Cys^{13}][45] and cyclic peptides possessing the Arg-Arg-Nal sequence, such as **2** and **3**, showed high CXCR4-antagonistic activity, we designed and separately prepared disulfide-bridged cyclic peptide libraries consisting of the *N*-3-guanidinopropanoyl-L/D-Cys(S-)-L/D-Arg-L/D-Nal-L/D-Cys-(S-)-NH_2 (or −tyramine) sequence, which included 32 compounds (2 × 2^4 stereoisomers) (**15a−p** or **16a−p**, respectively, Scheme 3). Among these synthetic compounds, **15e** [*N*-3-guanidinopropanoyl-Cys(S-)-Arg-Nal-D-Cys(S-)-NH_2] and **16e** [*N*-3-guanidinopropanoyl-Cys-(S-)-Arg-Nal-D-Cys(S-)-tyramine] exhibited moderate CXCR4-antagonistic activity (IC_{50} = 690 and 530 nM, respectively) (Table 1), although the other compounds did not show any activity up to the concentration of 1 μM. **15e** and **16e** have a common combination of chiralities of composed amino acids, suggesting that these compounds form similar conformations. It seems that a phenol group of **16e** is not disposed in the suitable position, since **15e** and **16e** have almost the same potencies. However, notably, L,L-chiralities of Arg-Nal are critical for high activity, as shown in **2** and **3**. The synthetic Arg side chain involving an *N*-3-guanidinopropanoyl moiety has an extra atom, compared to the original Arg side chain. This might account for the lower activity.

In addition, **15e/16e** analogues, **15q** and **16q**, in which the amide bond of *N*-3-guanidinopropanoyl-Cys was replaced by a reduced amide bond, and **15r** and **16r**, in which the α-amino group of Arg was N-methylated, were prepared. Substitution of the reduced amide bond for the amide bond of *N*-3-guanidinopropanoyl-Cys brought about no significant difference in potency (IC_{50} of **15q** and **16q** = c.a. 1 μM). This suggested that the planar character of this amide bond and the carbonyl group have little effect on potency. N-Methylation of Arg caused remarkable decrease in potency (IC_{50} of **15r** and **16r** > 10 μM), indicating that conformation surrounded by the Cys-Arg amide bond might be changed or the Cys-Arg amide proton might be required for high activity.

Olefin-Bridged Cyclic Peptides. Cyclic analogues that were bridged by an olefin instead of a disulfide in **15e** and **16e** were synthesized. C-Terminal-amidated compounds, **20a-c**, which differ in bridge length, and a C-terminal tyramide-type compound, **20d**, showed lower activity (IC_{50} = 1−10 μM), compared to those of **15e** and **16e** (Table 1). It is thought that the constraint of the olefin unit into the *E*-form is not an effective optimization component.

Analogues Constrained in the Peripheral Region of Arg^4. The significant difference of activity between **23e** ([Ala^4]-**2**, Ala-substitution for Arg^4, IC_{50} = 63 nM) and **23c** ([D-Ala^4]-**2** = [D-Ala^4]-**3**, D-Ala-substitution for L/D-Arg^4, IC_{50} = 230 nM) indicates a biological importance of the amide bond direction between D-Tyr and L/D-Arg. Thus, relationships between the conformation surrounded by Arg^4 of **2** and activity were investigated. L/D-Pro-substitutions for Arg^4 also gave the difference of activity: An L-Pro-substituted analogue, **23b**, is 4-fold stronger than a D-Pro-substituted analogue, **23a** (Table 2). N-Methylation of D-Ala^4 in **23c** (IC_{50} = 230 nM) brought about a significant increase in potency (IC_{50} of **23d** = 42 nM), which was comparable to that of **23e** ([Ala^4]-**2**) (IC_{50} = 63 nM), while N-methylation of Ala^4 in **23e** caused a significant decrease in potency (IC_{50} of **23f** = 490 nM). NMR and simulated annealing molecular dynamics (SA-MD) analysis showed that the backbone structure of **23d** is very similar to that of **23e**, but different from that of **23c**, especially in the direction of the D-Tyr-L/D-Arg amide bond (Figure 3A).[46] N-Methylation of D-Ala^4 in **23c** might cause an inversion of the D-Tyr^3-D-Ala^4 amide bond (180° rotation of ϕ and ψ torsion angles) to reduce the 1,3-pseudo-allylic strain between the side chain of D-Tyr^3 and the *N*-methyl group, resulting in a conformation that is similar to that of **23e**.

Ala-substitution for Arg^4 in **2** (**23e**) did not bring about a severe decrease in potency (IC_{50} = 63 nM),

Table 2. Inhibitory Activity of Cyclic Pentapeptides with Substitution for Arg[4] in Compound 2 against SDF-1 Binding to CXCR4

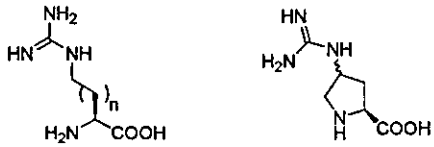

n = 1 γ-*N*-amidino-Dab (g-Dab)
n = 3 ε-*N*-amidino-Lys (g-Lys)

trans/*cis*-4-guanidino-Pro

compd	sequence[a]	$IC_{50} \pm SD$ (μM)
23a	*cyclo*(-Nal-Gly-D-Tyr-D-Pro-Arg-)	1.6 ± 0.1
23b	*cyclo*(-Nal-Gly-D-Tyr-Pro-Arg-)	0.42 ± 0.29
23c	*cyclo*(-Nal-Gly-D-Tyr-D-Ala-Arg-)	0.23 ± 0.0064
23d	*cyclo*(-Nal-Gly-D-Tyr-D-MeAla-Arg-)	0.042 ± 0.0088
23e	*cyclo*(-Nal-Gly-D-Tyr-Ala-Arg-)	0.063 ± 0.013
23f	*cyclo*(-Nal-Gly-D-Tyr-MeAla-Arg-)	0.49 ± 0.090
23g	*cyclo*(-Nal-Gly-D-Tyr-Dab-Arg-)	0.016 ± 0.010
23h	*cyclo*(-Nal-Gly-D-Tyr-Orn-Arg-)	0.019 ± 0.011
23i	*cyclo*(-Nal-Gly-D-Tyr-Lys-Arg-)	0.097 ± 0.0035
23j	*cyclo*(-Nal-Gly-D-Tyr-g-Dab-Arg-)	0.024 ± 0.0040
23k	*cyclo*(-Nal-Gly-D-Tyr-g-Lys-Arg-)	0.033 ± 0.0001
23l	*cyclo*(-Nal-Gly-D-Tyr-Asn-Arg-)	0.27
23m	*cyclo*(-Nal-Gly-D-Tyr-Gln-Arg-)	0.17
23n	*cyclo*(-Nal-Gly-D-Tyr-Glu-Arg-)	0.61
23o	*cyclo*(-Nal-Gly-D-Tyr-*trans*-4-guanidino-Pro-Arg-)	0.010 ± 0.0015
23p	*cyclo*(-Nal-Gly-D-Tyr-*cis*-4-guanidino-Pro-Arg-)	0.0099 ± 0.0043

[a] MeAla = N^{α}-Me-Ala.

whereas Ala-substitution for Nal[1], D-Tyr[3], and Arg[5] completely deminished activity of the parent compound (IC_{50} > 1 μM, data not shown). These results suggest that the side chain of Arg[4] in **2** has relatively little effect on the expression of activity, and that the spatial disposition of the δ-guanidino group of Arg[4] might not be optimized. Thus, several analogues, in which Arg[4] was replaced by Arg/Lys mimetics with various lengths of alkyl chains, were synthesized. Dab/L-ornithine (Orn)-substituted analogues, **23g** and **23h**, showed higher activity (IC_{50} = 16 and 19 nM, respectively) than the Ala-substituted analogue, **23e**, whereas a Lys-substituted analogue, **23i**, was slightly weaker (IC_{50} = 97 nM) than **23e** (Table 2). γ-*N*-Amidino-Dab (g-Dab)/ε-*N*-amidino-Lys (g-Lys)-substituted analogues, **23j** and **23k**, also showed higher activity (IC_{50} = 24 and 33 nM, respectively) than **23e**. However, these analogues were weaker than compound **2**, suggesting that Arg is the most suitable at position 4 among the Arg/Lys mimetics used in this study. Asn/Gln/Glu-substituted analogues, **23l**–**n**, showed a remarkable decrease in activity (IC_{50} = 270, 170, and 610 nM, respectively). This proved that a basic functional group, such as an amino or guanidino group, is necessary for strong activity in the side chain of the amino acid at position 4, and that a hydrophilic (not basic) or acidic group is not preferable to a methyl group of Ala.

Conformationally constrained Arg mimetics, *trans*-4-guanidino-Pro and *cis*-4-guanidino-Pro (Table 2), were synthesized with the idea of fixing the backbone and side chain of Arg, according to the reported procedure.[44] These Arg mimetics were incorporated in compound **2** to determine the spatial disposition of guanidino group and increase in potency. **23o** ([*trans*-4-guanidino-Pro[4]]-**2**, *trans*-4-guanidino-Pro-substitution for Arg[4]) and **23p** ([*cis*-4-guanidino-Pro[4]]-**2**, *cis*-4-guanidino-Pro-substitution for Arg[4]) showed high CXCR4-antagonistic activities (IC_{50} = 10 and 9.9 nM, respectively) that were twice as strong as that of **23j** ([g-Dab[4]]-**2**, g-Dab-substitution for Arg[4]), having the same length of the linear-type side chain of the amino acid at position 4 (IC_{50} = 24 nM), while **23b** ([Pro[4]]-**2**, Pro-substitution for Arg[4]) did not show high activity (IC_{50} = 420 nM). In consideration of the fact that the introduction of a pyrrolidinyl ring caused a significant reduction of potency (**23a** and **23b**), it is thought that fixing the side chain effectively increased potency. From these results, we have learned that the constrained guanido group might efficiently interact with CXCR4. In addition, NMR and SA-MD analysis of **23o** and **23p** showed similar dispositions of guanidino groups of *trans*/*cis*-4-guanidino-Pro residues in space (Figure 3B),[46] which might be the reason for essentially no difference in potency between **23o** and **23p**.

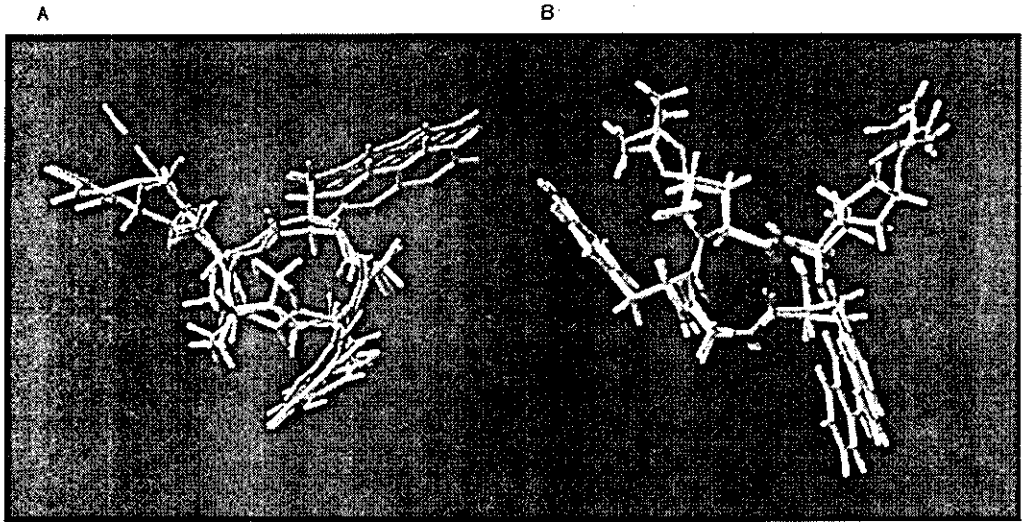

Figure 3. Superimpositions of low-energy structures of **23c** (red), **23d** (green), and **23e** (blue) (A), and **23o** and **23p** (B).

Conclusion

The fine-tuning of the ring structure of compound **2** led to findings of CXCR4 antagonists involving scaffold structures that are different from cyclic pentapeptide structures: A cyclic tetrapeptide including a γ-amino acid and pseudopeptides cyclized by disulfide and olefin bridges, having a smaller number of peptide bonds compared to compound **2**, might be useful lead compounds. Furthermore, we have learned from L/D-N^{α}-Me-Ala- and L/D-Pro-substitutions for Arg^4 that the direction of the carbonyl group in the D-Tyr^3-L/D-Ala^4 amide bonds causes a remarkable effect on CXCR4-antagonistic activity. It is also clear from this study that a basic functional group, such as amino or guanidino group, in the amino acid side-chain at position 4 is indispensable for strong activity. In addition, analogues of compound **2**, where a conformationally constrained Arg mimetic, trans- or *cis*-4-guanidino-Pro, was incorporated at position 4, showed high CXCR4-antagonistic activity, indicating that spatial constraint of a guanido group is important for an efficient interaction with CXCR4. These results for modifications of compound **2** provide useful insights for the future design of new low molecular weight CXCR4 antagonists, considering in connection with other CXCR4 antagonists.[47-53]

Experimental Section

General. ^{1}H NMR spectra were recorded using a JEOL EX-270, a JEOL AL-400, or a JNM-ECA600 spectrometer at 270, 400, or 600 MHz ^{1}H frequency, respectively, in $CDCl_3$ or DMSO-d_6. Chemical shifts are reported in parts per million downfield from internal tetramethylsilane. Nominal (LRMS) and exact mass (HRMS) spectra were recorded on a JEOL JMS-01SG-2 or JMS-HX/HX 110A mass spectrometer. Ionspray (IS)-mass spectrum was obtained with a Sciex API*III*E triple quadrupole mass spectrometer (Toronto, Canada). Optical rotations were measured in $CHCl_3$ or H_2O with a JASCO DIP-360 digital polarimeter (Tokyo, Japan) or a Horiba high-sensitive polarimeter SEPA-200 (Kyoto, Japan). For flash column chromatography, silica gel 60 H (silica gel for thin-layer chromatography, Merck) and Wakogel C-200 (silica gel for column chromatography, Wako Pure Chemical Industries, Ltd., Osaka, Japan) were employed. HPLC solvents were H_2O and CH_3CN, both containing 0.1% (v/v) TFA. For analytical HPLC, a Cosmosil 5C18-AR column (4.6 × 250 mm, Nacalai Tesque Inc., Kyoto, Japan) was eluted with a linear gradient of CH_3CN at a flow rate of 1 mL/min on a Waters model 600 (Nihon Millipore, Ltd., Tokyo, Japan). Preparative HPLC was performed on a Waters Delta Prep 4000 equipped with a Cosmosil 5C18-AR column (20 × 250 mm, Nacalai Tesque Inc.) using an isocratic mode of CH_3CN at a flow rate of 15 mL/min.

[1-(*N*,*N*-Methoxy-methyl-carbamoyl)-2(*S*)-(2-naphthyl)-ethyl]-carbamic Acid *tert*-Butyl Ester (Boc-Nal-NMe (OMe)) (4). To a stirred solution of L-3-(2-naphthyl)alanine (10.0 g, 46.4 mmol) in THF−H_2O (1:1 (v/v), 200 mL) were added triethylamine (12.5 mL, 92.9 mmol) and Boc_2O (9.63 g, 44.1 mmol) at room temperature, and the mixture was stirred at this temperature overnight. The reaction mixture was concentrated under reduced pressure. The residue was extracted with EtOAc, and the extract was washed successively with saturated aqueous citric acid, aq. 5% citric acid (× 3), H_2O (× 5), and brine and dried over $MgSO_4$. Concentration under reduced pressure gave the crude product as a white powder, which was used directly in the following step without purification. To a solution of the crude product in DMF (150 mL) were added *N*,*O*-dimethylhydroxylamine hydrochloride (10.3 g, 106 mmol), triethylamine (14.3 mL, 106 mmol), HOBt (8.11 g, 52.9 mmol), and DCC (11.8 g, 53.0 mmol) at 0 °C, and the mixture was stirred at room temperature overnight. The reaction mixture was filtered, and the filtrate was concentrated under reduced pressure. The residue was extracted with EtOAc, and the extract was washed successively with saturated aqueous citric acid, brine, saturated aqueous $NaHCO_3$, and brine and dried over $MgSO_4$. Concentration under reduced pressure followed by flash chromatography over silica gel with EtOAc−*n*-hexane (2:3) and subsequent recrystalization with Et_2O−*n*-hexane gave 12.8 g (35.7 mmol, 77% yield from L-3-(2-naphthyl)alanine) of **4** as colorless crystals. mp: 110−111 °C; $[\alpha]^{35}_D$ +29.41 (*c* 0.714, $CHCl_3$); ^{1}H NMR (400 MHz, $CDCl_3$) δ 7.73-7.82 (m, 3H), 7.62, (s, 1H), 7.39−7.48 (m, 2H), 7.31 (dd, *J* = 8.6, 1.5 Hz, 1H), 5.17−5.24 (br d, 1H), 5.06 (br, 1H), 3.66 (s, 3H), 3.01−3.25 (m, 4H), 1.36 (s, 9H); Anal. Calcd for $C_{20}H_{25}N_2O_6$: C, 67.02; H, 7.31; N, 7.82. Found: C, 66.78; H, 7.47; N, 7.68.

(2*E*,4*S*)-*N*-Boc-4-amino-5-(2-naphthyl)-2-pentenoic Acid *tert*-Butyl Ester (5). To a stirred solution of **4** (7.00 g, 19.5 mmol) in CH_2Cl_2 (50 mL) was added dropwise a solution of DIBAL-H in toluene (1.0 M, 38.6 mL, 38.6 mmol) at −78 °C under argon, and the mixture was stirred at −78 °C for 2 h. The reaction was quenched with saturated aqueous citric acid (50 mL) at −78 °C, and the organic solvents were concentrated under reduced pressure. The residue was extracted with EtOAc, and the extract was washed successively with brine, aq. 50% $NaHCO_3$, and brine and dried over $MgSO_4$. Concentration under reduced pressure gave the crude aldehyde as a white solid, which was used directly in the following step without purification. To a stirred suspension of LiCl (1.65 g, 39.0 mmol) in CH_3CN (30 mL) were added $(EtO)_2P(O)CH_2CO_2$-Bu^t (6.31 mL, 39.0 mmol) and DIPEA (6.79 mL, 39.0 mmol) at 0 °C under argon, and the mixture was stirred at 0 °C for 1 h. The above aldehyde in CH_3CN (30 mL) was added to the mixture at 0 °C, and the mixture was allowed to warm to room temperature and stirred overnight. The reaction mixture was concentrated under reduced pressure. The residue was extracted with EtOAc, and the extract was washed successively with saturated aqueous citric acid, brine, saturated aqueous $NaHCO_3$, and brine and dried over $MgSO_4$. Concentration under reduced pressure followed by flash chromatography over silica gel with EtOAc−*n*-hexane (1:4) and subsequent recrystalization with Et_2O−*n*-hexane gave 6.05 g (15.2 mmol, 78% from **4**) of **5** as colorless crystals. mp: 135−137 °C; $[\alpha]^{35}_D$ −12.84 (*c* 0.467, $CHCl_3$); ^{1}H NMR (400 MHz, $CDCl_3$) δ 7.72−7.87 (m 3H), 7.62 (s, 1H), 7.39−7.51 (m, 2H), 7.31 (dd, *J* = 8.6, 1.7 Hz, 1H), 6.85 (dd, *J* = 15.6, 5.1 Hz, 1H), 5.81 (dd, *J* = 15.6, 1.5 Hz, 1H), 4.69 (br, 1H), 4.57 (br, 1H), 2.94−3.12 (m, 2H), 1.46 (s, 9H), 1.36 (s, 9H); Anal. Calcd for $C_{24}H_{31}NO_4$: C, 72.58; H, 7.86; N, 3.52. Found: C, 72.44; H, 7.86; N, 3.22.

(2*E*,4*S*)-*N*-Fmoc-4-amino-5-(2-naphthyl)-2-pentenoic Acid (6). **5** (1.00 g, 2.51 mmol) was treated with aq. 95% TFA (20 mL) at room temperature for 2.5 h. TFA was removed under reduced pressure, and the residue was dissolved in DMF−H_2O−CH_3CN (9:1:15 (v/v), 24 mL). To the stirred solution were added DIPEA (876 μL, 5.03 mmol) and Fmoc-OSu (891 mg, 2.64 mmol) at 0 °C, and the reaction mixture was stirred at room temperature for 6 h. The mixture was concentrated under reduced pressure and acidified with aq. 1 M HCl. The mixture was extracted with EtOAc, and the extract was washed successively with aq. 0.1 M HCl (× 3) and brine and dried over $MgSO_4$. After removal of the solvent under reduced pressure, the resulting crude product was purified by flash chromatography on silica gel with $CHCl_3$−MeOH (20:1) and subsequent recrystalization with ($CHCl_3$−*n*-hexane−MeOH) to give 345.1 mg (0.753 mmol, 30% yield from **5**) of **6** as colorless crystals. mp: 189−190 °C; $[\alpha]^{34}_D$ −15.33 (*c* 0.326, $CHCl_3$); ^{1}H NMR (400 MHz, DMSO-d_6) δ 12.3 (br, 1H), 7.67−7.95 (m, 7H), 7.51−7.62 (m, 2H) 7.40−7.51 (m, 3H), 7.30−7.41 (m, 2H) 7.08−7.30 (m, 2H), 6.86 (dd, *J* = 15.6, 5.4 Hz, 1H), 5.81 (d, *J* = 15.6 Hz,1H), 4.43−4.61 (m, 1H), 4.04−4.26 (m, 3H), 3.00−3.14 (m, 1H), 2.83−3.00 (m, 1H); LRMS (FAB), *m/z* 464 (MH^+, base peak), 307, 179, 165, 154, 136, 141, 136, 121, 107, 91, 89, 77; HRMS (FAB), *m/z* calcd for $C_{30}H_{26}NO_4$ (MH^+): 464.1862, found: 464.1853.

***N*-Boc-4(*R*)-amino-5-(2-naphthyl)-pentanoic Acid *tert*-Butyl Ester (7).** To the solution of **5** (2.50 g, 6.29 mmol) in

EtOAc (100 mL) was added 10% Pd/C (200 mg). The reaction vessel was charged with atmosphere of H_2 (balloon), and the mixture was stirred at room temperature for 8 h. Completion of the reaction was monitored by RP-HPLC. The reaction mixture was filtered through a pad of Celite, rinsing with EtOAc, and the filtrate was concentrated under reduced pressure. The resulting crude product was purified by flash chromatography on silica gel with EtOAc–*n*-hexane (1:5) and subsequent recrystalization with Et_2O–*n*-hexane to give 1.87 g (4.65 mmol, 74%) of **7** as colorless crystals. mp: 90–91 °C; $[\alpha]^{35}_D$ −20.83 (*c* 0.432, $CHCl_3$); ^1H NMR (400 MHz, $CDCl_3$) δ 7.71–7.86 (m, 3H), 7.62 (s, 1H), 7.38–7.52 (m, 2H), 7.34 (d, J = 8.1 Hz, 2H), 4.42–4.58 (br d, 1H), 2.94–3.09 (m, 1H), 2.79–2.94 (m, 1H), 2.28 (t, 2H), 1.56–1.92 (m, 2H), 1.41 (s, 9H), 1.39 (s, 9H); Anal. Calcd for $C_{24}H_{33}NO_4$: C, 72.15; H, 8.33; N, 3.51. Found: C, 71.92; H, 8.49; N, 3.21.

N-Fmoc-4(*R*)-amino-5-(2-naphthyl)-pentanoic Acid (8). **7** (1.00 g, 2.50 mmol) was treated with aq. 95% TFA (20 mL) at room temperature for 2.5 h. TFA was removed under reduced pressure, and the residue was dissolved in DMF–H_2O–THF (9:1:10 (v/v), 20 mL). To the stirred solution were added DIPEA (1.03 mL, 5.89 mmol) and Fmoc-OSu (1.29 g, 3.83 mmol) at 0 °C, and the reaction mixture was stirred at room temperature overnight. The mixture was concentrated under reduced pressure and acidified with aq. 1 M HCl. The mixture was extracted with EtOAc, and the extract was washed successively with aq. 0.1 M HCl (× 3) and brine and dried over $MgSO_4$. After removal of the solvent under reduced pressure, the resulting crude product was purified by flash chromatography on silica gel with $CHCl_3$–MeOH (20:1) and subsequent recrystalization with ($CHCl_3$–*n*-hexane) to give 747.6 mg (1.60 mmol, 64% yield from **7**) of **8** as colorless crystals. mp: 167–169 °C; $[\alpha]^{34}_D$ −7.31 (*c* 0.410, $CHCl_3$); ^1H NMR (400 MHz, DMSO-d_6) δ 7.73–7.92 (m 5H), 7.67 (s, 1H), 7.56–7.62 (m, 2H) 7.41–7.48 (m, 2H), 7.33–7.41 (m, 3H), 7.18–7.33 (m, 3H), 4.06–4.24 (m, 3H), 3.76 (br, 1H), 2.85 (d, J = 6.6 Hz, 2H), 2.14–2.32 (m, 2H), 1.68–1.82 (m, 1H), 1.54–1.68 (m, 1H); LRMS (FAB), *m/z* 466 (MH^+, base peak), 179, 154, 136, 141, 136; HRMS (FAB), *m/z* calcd for $C_{30}H_{28}NO_4$ (MH^+): 466.2018, found: 464.2024.

Representative Procedure for the Synthesis of γ-Amino Acid-Containing Cyclic Tetrapeptides (11a). Cl-Trt(2-Cl) resin (1.25 mmol/g, 400 mg, 0.5 mmol) was treated with Fmoc-γ-Nal-OH (256 mg, 0.55 mmol) and DIPEA (383 μL, 2.2 mmol) in CH_2Cl_2 (4 mL) at room temperature for 2 h to yield Fmoc-γ-Nal-Trt(2-Cl) resin (0.79 mmol/g, 97%). Protected peptide **11a** resin was manually constructed by Fmoc-based solid-phase peptide synthesis on Fmoc-γ-Nal-Trt(2-Cl) resin (0.79 mmol/g, 127 mg, 0.1 mmol). Bu^t for Tyr and Pbf for Arg were employed for side-chain protection. The protected peptide **11a** resin was treated with 1,1,1,3,3,3-hexafluoro-2-propanol (HFIP)–DCM (1:4 (v/v), 7 mL) at room temperature for 2 h. After filtration, the filtrate was concentrated under reduced pressure to give the crude protected linear peptide. To a stirred mixture of the protected peptide and *N*-methylmorphorine (54.9 μL, 0.5 mmol) in DMF (25 mL) was added diphenylphosphoryl azide (DPPA) (53.2 μL, 0.247 mmol) at −40 °C. The reaction mixture was stirred for 24 h with warming up to room temperature and concentrated under reduced pressure. The residue was subjected to solid-phase extraction over basic alumina in $CHCl_3$–MeOH (9:1) to remove inorganic salts derived from DPPA. The resulting cyclic protected peptide was treated with aq. 95% TFA (10 mL) at room temperature for 2 h. Concentration under reduced pressure and purification by HPLC gave the cyclic pseudopeptide **11a** (42.9 mg, 61% yield from Fmoc-γ-Nal-Trt(2-Cl) resin) as a freeze-dried powder.

Fmoc-tyramine-Wang PEG Resin. To a mixture of Wang PEG resin (0.33 mmol/g, 1.82 g, 0.600 mmol), Fmoc-tyramine (647 mg, 1.80 mmol), Ph_3P (472 mg, 1.80 mmol), and *N*-methylmorphorine (66.0 μL, 0.600 mmol) in CH_2Cl_2–THF (3:1 (v/v), 16 mL) was added diisopropyl azodicarboxylate (DIAD) (40% solution in toluene, 886 μL, 1.80 mmol) at 0 °C. The reaction mixture was stirred at room temperature for 2 d. The obtained resin was washed with THF (20 mL × 3), DMF (20 mL × 3), MeOH (20 mL × 3), $CHCl_3$ (20 mL × 3) and Et_2O (20 mL × 3) and dried in vacuo. The loading rate of the resin was estimated by Fmoc-quantification (0.126 mmol/g (41%)).

Representative Procedure for the Synthesis of Disulfide-Bridged Cyclic Peptides (16e). Protected peptide resin was manually constructed by Fmoc-based solid-phase peptide synthesis on Fmoc-tyramine-Wang PEG resin (0.126 mmol/g, 397 mg, 0.05 mmol). Fmoc-β-Ala-OH was condensed to the N-terminal amino group of H-Cys-Arg(Pbf)-Nal-D-Cys-tyramine-Wang PEG resin, and Fmoc group was deprotected by treatment with 20% piperidine in DMF (20 min). To a mixture of the resin and DIPEA (52,5 μL, 0.300 mmol) in DMF (5 mL) was added 1*H*-pyrazole-1-carboxamidine hydrohloride (22.0 mg, 0.150 mmol) at room temperature. The reaction mixture was stirred at room temperature for 12 h. This N-guanylation procedure was repeated once again. The protected resin was treated with EDT/H_2O/TFA (2.5:2.5:95 (v/v), 6 mL) at 0 °C for 2 h. The reaction mixture was filtered, and the filtrate was concentrated by bubbling with N_2 gas. Cooled Et_2O was added to the residue, and the resulting precipitate was separated by centrifugation. The precipitate was washed with Et_2O three times. The crude peptide was dissolved in H_2O, and pH of this solution was adjusted to approximately 8 with aq. 0.28% NH_3. Air oxidation for 1 d and purification by HPLC gave the cyclic pseudopeptide **16e** (6.5 mg, 16% yield from Fmoc-tyramine-Wang PEG resin) as a freeze-dried powder.

Synthesis of 15q. Protected peptide resin was manually constructed by Fmoc-based solid-phase peptide synthesis on Fmoc-HN-Rink amide resin (0.36 mmol/g, 139 mg, 0.05 mmol). To a suspension of H-Cys-Arg(Pbf)-Nal-D-Cys-HN-Rink amide resinin DCM were added *N*-Fmoc-3-aminopropanal (44.0 mg, 0.15 mmol) and $NaBH(OAc)_3$ (53.0 mg, 0.25 mmol) at room temperature. The mixture was stirred at room-temperature overnight. Deprotection of the Fmoc group, N-guanylation, deprotection/cleavage from the resin, air oxidation, and HPLC purification were performed by use of a procedure identical with that described for the synthesis of **16e** to yield the cyclic pseudopeptide **15q** (3.0 mg, 9% yield from Fmoc-HN-Rink amide resin) as a freeze-dried powder.

Representative Procedure for the Synthesis of Olefin-Bridged Cyclic Peptides (20a). Protected peptide resin was manually constructed by Fmoc-based solid-phase peptide synthesis on Fmoc-HN-Rink amide resin (0.29 mmol/g, 172 mg, 0.05 mmol). Fmoc-β-Ala-OH was condensed to the N-terminal amino group of H-L-2-allylGly-Arg(Pbf)-Nal-D-2-allylGly-HN-Rink amide resin. To a suspension of the protected resin in dry DCM (5 mL) was added Grubbs catalyst second generation (4.20 mg, 5.00 μmol) at room temperature under argon. The reaction mixture was refluxed for 9 h. After removal of the organic solvent, this reaction was repeated once again for 12 h in the presence of the catalyst (21 mg, 0.025 mmol) in dry DCM (5 mL). The obtained resin was treated with 20% piperidine in DMF (20 min). To a mixture of the resin and DIPEA (52.5 μL, 0.300 mmol) in DMF was added 1*H*-pyrazole-1-carboxamidine hydrohloride (22.0 mg, 0.15 mmol) at room tempereture. The reaction mixture was stirred at room temperature for 12 h. This N-guanylation procedure was repeated once again. The protected resin was treated with thioanisole (940 μL), TFA (7.2 mL), and TMSBr (1.32 mL) at 0 °C for 2 h. The reaction mixture was filtered, and the filtrate was concentrated by bubbling with N_2 gas. Cooled Et_2O was added to the residue, and the resulting precipitate was separated by centrifugation. The precipitate was washed with Et_2O. The crude peptide was purified by HPLC to give the cyclic pseudopeptide **20a** (3.3 mg, 10% yield from Fmoc-HN-Rink amide resin) as a freeze-dried powder.

Representative Procedure for the Synthesis of Cyclic Pentapeptides (*cyclo*(-D-Tyr-Pro-Arg-Nal-Gly-) (23b)). Protected peptide resin was manually constructed by Fmoc-based solid-phase peptide synthesis on Fmoc-Gly-Trt(2-Cl) resin (0.741 mmol/g, 101 mg, 0.075 mmol). Bu^t for Tyr and Pbf for Arg were employed for side-chain protection. Cleavage from the resin, cyclization, deprotection, and HPLC purification were performed by use of a procedure identical with that

described for the synthesis of **11a** to yield the cyclic peptide **23b** (25.2 mg, 50% yield from Fmoc-Gly-Trt(2-Cl) resin) as a freeze-dried powder.

Representative Procedure for the Synthesis of *N*-Methylated Cyclic Pentapeptides (*cyclo*(-D-Tyr-D-MeAla-Arg-Nal-Gly-) (23d)). According to a procedure identical with that described for the preparation of **23b**, **23d** was synthesized except for N-methylation of the D-Ala residue. N-Methylation was performed by the Fukuyama–Mitsunobu reaction:[28] To a mixture of H-D-Ala-Arg(Pbf)-Nal-Gly-Trt(2-Cl) resin (0.075 mmol) and *o*-nitrobenzenesulfonyl chloride (49.9 mg, 0.225 mmol) in CH_2Cl_2 (5 mL) was added 2,4,6-collidine (49.6 μL, 0.375 mmol) at room temperature. The reaction mixture was stirred at room temperature for 2 h, and the resin was washed successively with CH_2Cl_2 (10 mL × 3) and DMF (10 mL × 3). To a mixture of the resin, Ph_3P (98.4 mg, 0.375 mmol), and MeOH (15.2 μL, 0.375 mmol) in dry THF (5 mL) was added diethyl azodicarboxylate (DEAD) (40% solution in toluene, 170 μL, 0.375 mmol) at 0 °C. The reaction mixture was stirred at room temperature for 2 h. The resin was washed successively with THF (10 mL × 3) and DMF (10 mL × 3). To a mixture of the resin and DBU (56.1 μL, 0.375 mmol) in DMF (5 mL) was added 2-mercaptoethanol (51.4 μL, 0.750 mmol) at room temperature, and the reaction mixture was stirred at room temperature for 2 h. Subsequent condensation of the next residue (D-Tyr) to the secondary amino group on the resin was performed by treatment with Fmoc-D-Tyr(Bu^t)-OH (5 equiv), HATU (4.9 equiv), HOAt (5 equiv), and DIPEA (10 equiv) in DMF (5 mL) for 1 h (× 2). **23d** (freeze-dried powder): 3.0 mg, 6.0% yield from Fmoc-Gly-Trt(2-Cl) resin.

(2*S*,4*S*)-*N*$^\alpha$-Cbz-4-*N*-Boc-aminoproline Benzyl Ester. (2*S*,4*S*)-*N*$^\alpha$-Cbz-4-aminoproline benzyl ester (1.44 g, 3.93 mmol), which was prepared from (2*S*,4*S*)-*N*$^\alpha$-Cbz-4-azidoproline benzyl ester according to Tamaki's procedure,[35] was dissolved in THF (20 mL), and Boc_2O (1.38 g, 6.31 mmol) and triethylamine (1.10 mL, 7.89 mmol) were added to the solution at 0 °C. The reaction mixture was stirred at room temperature for 7.5 h. The mixture was concentrated under reduced pressure, and the residue was extracted with Et_2O. The extract was washed successively with saturated aqueous citric acid (× 2), H_2O (× 2), and brine and dried over $MgSO_4$. After removal of the solvent under reduced pressure, the resulting crude product was purified by flash chromatography on silica gel with EtOAc–*n*-hexane (1:4) to give 1.70 g (3.77 mmol, 96% yield) of the title compound as a colorless oil. $[\alpha]^{29}_D$ −39.47 (*c* 0.304, $CHCl_3$); ^{1}H NMR (400 MHz, $CDCl_3$) δ 7.18–7.45 (m, 10H), 4.95–5.40 (m, 5H), 4.28–4.50 (m, 2H), 3.68–3.82 (m, 1H), 3.44–3.60 (m, 1H), 2.39–2.57 (m, 1H), 1.89–2.05 (m, 1H), 1.45 (s, 9H); LRMS (FAB), *m/z* 477 (MNa^+, base peak), 455 (MH^+), 445, 399, 355, 91; HRMS (FAB), *m/z* calcd for $C_{25}H_{31}N_2O_6$ (MH^+): 455.2182, found: 455.2186.

(2*S*,4*S*)-*N*$^\alpha$-Fmoc-4-*N*-Boc-aminoproline. (2*S*,4*S*)-*N*$^\alpha$-Cbz-4-*N*-Boc-aminoproline benzyl ester (1.70 g, 3.77 mmol) was dissolved in EtOH (80 mL), and 5% Pd/C (170 mg) was added to the solution. The reaction vessel was charged with atmosphere of H_2 (balloon), and the mixture was stirred at room temperature for 12 h. After removal of Pd/C by filtration, the filtrate was concentrated under reduced pressure to give the crude product as a colorless oil, which was used directly in the following step without purification. To the crude product in H_2O–THF (4:3 (v/v), 70 mL) were added triethylamine (1.41 mL, 7.55 mmol) and Fmoc-OSu (2.54 g, 7.55 mmol) in CH_3CN (10 mL) at 0 °C, and the reaction mixture was stirred at room temperature for 2 h. The mixture was acidified with saturated aqueous citric acid and concentrated under reduced pressure. The residue was extracted with EtOAc, and the extract was washed successively with saturated aqueous citric acid, H_2O (× 3), and brine and dried over $MgSO_4$. After removal of the solvent under reduced pressure, the resulting crude product was purified by flash chromatography on silica gel with $CHCl_3$–MeOH (20:1) to give 1.18 g (2.60 mmol, 69% yield) of the title compound as colorless crystals. mp: 87–89 °C; $[\alpha]^{24}_D$ −33.81 (*c* 0.621, $CHCl_3$); ^{1}H NMR (400 MHz, DMSO-d_6) δ 8.30 (s, 1H), 7.82–7.97 (m, 2H), 7.57–7.75 (m, 2H), 7.25–7.49 (m, 4H), 3.93–4.36 (m, 5H), 3.60–3.75 (m, 1H), 3.05–3.21 (m, 1H), 2.32–2.58 (m, 1H), 1.67–1.90 (m, 1H), 1.44 (s, 9H); LRMS (FAB), *m/z* 451 [$(M - H)^-$], 229, 155, 153, 152 (base peak); HRMS (FAB), *m/z* calcd for $C_{25}H_{27}N_2O_6$ [$(M - H)^-$]: 451.1868, found: 451.1883.

(2*S*,4*R*)-*N*$^\alpha$-Cbz-4-*N*-Boc-aminoproline Benzyl Ester. By use of a procedure identical with that described for the preparation of (2*S*,4*S*)-*N*$^\alpha$-Cbz-4-*N*-Boc-aminoproline benzyl ester, (2*S*,4*R*)-*N*$^\alpha$-Cbz-4-aminoproline benzyl ester (5.56 g, 15.7 mmol) was converted into 6.24 g (13.8 mmol, 88% yield) of the title compound as colorless crystals. mp: 97–99 °C; $[\alpha]^{25}_D$ −47.61 (*c*, 0.714, $CHCl_3$); ^{1}H NMR (400 MHz, $CDCl_3$) δ 7.15–7.43 (m, 10H), 4.93–5.27 (m, 4H), 4.56–4.70 (br, 1H), 4.37–4.54 (m, 1H), 4.21–4.35 (br, 1H), 3.78–3.89 (m, 1H), 3.30–3.50 (m, 1H), 2.12–2.34 (m, 2H), 1.45 (s, 9H); LRMS (FAB), *m/z* 477 (MNa^+, base peak), 455 (MH^+), 445, 399, 355, 263, 91; HRMS (FAB), *m/z* calcd for $C_{25}H_{31}N_2O_6$ (MH^+): 455.2182, found: 455.2176.

(2*S*,4*R*)-*N*$^\alpha$-Fmoc-4-*N*-Boc-aminoproline. By use of a procedure identical with that described for the preparation of (2*S*,4*S*)-*N*$^\alpha$-Fmoc-4-*N*-Boc-aminoproline, (2*S*,4*R*)-*N*$^\alpha$-Cbz-4-*N*-Boc-aminoproline benzyl ester (2.75 g, 6.10 mmol) was converted into 2.05 g (4.51 mmol, 74% yield) of the title compound as colorless crystals. mp: 85–87 °C; $[\alpha]^{24}_D$ −36.92 (*c* 0.325, $CHCl_3$); ^{1}H NMR (400 MHz, $CDCl_3$) δ 8.33 (s, 1H), 7.82–7.97 (m, 2H), 7.56–7.72 (m, 2H), 7.26–7.49 (m, 4H), 3.96–4.36 (m, 4H), 3.50–3.67 (m, 1H), 3.18–3.40 (m, 2H), 1.99–2.26 (m, 2H), 1.44 (s, 9H); LRMS (FAB), *m/z* 451 [$(M - H)^-$], 229, 155, 153, 151 (base peak); HRMS (FAB), *m/z* calcd for $C_{25}H_{27}N_2O_6$ [$(M - H)^-$]: 451.1868, found: 451.1887.

Representative Procedure for the Synthesis of Cyclic Pentapeptides Containing Arginine Mimetic (*cyclo*(-D-Tyr-*trans*-4-guanidino-Pro-Arg-Nal-Gly-) (23o)). According to a procedure identical with that described for the preparation of **23b**, the cyclic protected peptide was synthesized. The obtained protected peptide (0.05 mmol) was treated with aq. 95% TFA (5 mL) for 2 h at room temperature, and concentration under reduced pressure gave the crude cyclic peptide. To a mixture of the crude product and 1*H*-pyrazole-1-carboxamidine hydrochloride (22.0 mg, 0.15 mmol) in DMF (4 mL) was added DIPEA (52.3 μL, 0.300 mmol) at room temperature. The reaction mixture was stirred at room temperature for 12 h. This procedure (N-guanylation of the γ-amino group of the *trans*-4-amino-Pro residue) was repeated once again. Concentration under reduced pressure and purification by HPLC gave the cyclic peptide **23o** (5.1 mg, 14% yield from Fmoc-Gly-Trt(2-Cl) resin) as a freeze-dried powder.

[^{125}I]-SDF-1 Binding and Displacement. Stable CHO cell transfectants expressing CXCR4 variants were prepared as described previously.[54] CHO transfectants were harvested by treatment with trypsin-EDTA, allowed to recover in complete growth medium (MEM-α, 100 μg/mL penicillin, 100 μg/mL streptomycin, 0.25 μg/mL amphotericin B, 10% (v/v)) for four to 5 h and then washed in cold binding buffer (PBS containing 2 mg/mL BSA). For ligand binding, the cells were resuspended in binding buffer at 1×10^7 cells/mL, and 100 μL aliquots were incubated with 0.1 nM of [^{125}I]-SDF-1 (PerkinElmer Life Sciences) for 2 h on ice under constant agitation. Free and bound radioactivity were separated by centrifugation of the cells through an oil cushion and bound radioactivity was measured with a gamma-counter (Cobra, Packard, Downers Grove, IL). Inhibitory activity of test compounds was determined based on the inhibition of [^{125}I]-SDF-1-binding to CXCR4 transfectants (IC_{50}).

NMR Spectroscopy (23c–e, 23o, and 23p). The peptide sample was dissolved in DMSO-d_6 at a concentration of 5 mM. ^{1}H NMR spectra of the peptides were recorded at 300 K. The assignments of the proton resonances were achieved by use of ^{1}H–^{1}H COSY spectra. $^3J(H^N,H^\alpha)$ coupling constants were measured from one-dimensional spectra. The mixing time for the NOESY experiments was set at 400 ms. NOESY spectra were composed of 512 real points in the F2 dimension and 256 real points, which were zero-filled to 256 points in the F1 dimension, with 144 scans per t1 increment. The cross-peak

intensities were evaluated by relative build-up rates of the cross-peaks. Temperature dependence of the chemical shifts of all of the amide protons was investigated in **23c−e**, **23o**, and **23p**. In **23c**, the temperature coefficients for all of the NH protons were large. In **23d**, the only temperature coefficient for the NH of D-Tyr^3 was small, but NOE was not observed between the Nal^1 C$^\alpha$H and D-Tyr^3 NH. In **23e**, **23o**, and **23p**, the temperature coefficients for the NH of D-Tyr^3 and Arg^5 were small, but NOE was not observed between the Nal^1 C$^\alpha$H and D-Tyr^3 NH or between the D-Tyr^3 C$^\alpha$H and Arg^5 NH. Thus, no hydrogen bond restraints were used in the simulated annealing calculations of **23c−e**, **23o**, and **23p**.

Calculation of Structures. The structure calculations were performed on a Silicon Graphics Origin 2000 workstation with the NMR-refine program within the Insight II/Discover package using the consistent valence force field (CVFF).[55] Pseudoatoms were defined for the methylene protons of Nal^1, D-Tyr^3, Arg^4, and Arg^5 prochiralities of which were not identified by ^{1}H NMR data. The restraints, in which the Gly^2 α-methylene participated, were defined for the separate protons without definition of the prochiralities. The dihedral ϕ angle constraints were calculated based on the Karplus equation: $^3J(H^N,H^\alpha) = 6.7\cos^2(\theta - 60) - 1.3\cos(\theta - 60) + 1.5$.[56] Lower and upper angle errors were set to 15°. The NOESY spectrum with a mixing time of 400 ms was used for the estimation of the distance restraints between protons. The NOE intensities were classified into three categories (strong, medium, and weak) based on the number of contour lines in the cross-peaks to define the upper-limit distance restraints (2.7, 3.5, and 5.0 Å, respectively). The upper-limit restraints were increased by 1.0 Å for the involved pseudoatoms. Lower bounds between nonbonded atoms were set to their van der Waals radii (1.8 Å). These distance and dihedral angle restraints were included with force constants of 25−100 kcal/mol·Å^2 and 25−100 kcal/mol·rad^2, respectively. The 50 initial structures generated by the NMR refine program randomly were subjected to the simulated annealing calculations. The final minimization stage was achieved until the maximum derivative became less than 0.01 kcal/mol·Å^2 by the steepest descents and conjugate gradients methods.

Acknowledgment. This work was supported in part by a 21st Century COE Program "Knowledge Information Infrastructure for Genome Science", a Grant-in-Aid for Scientific Research from the Ministry of Education, Culture, Sports, Science and Technology, Japan, and the Japan Health Science Foundation. Computation time was provided by the Supercomputer Laboratory, Institute for Chemical Research, Kyoto University. S.U. is grateful for a Research Fellowship from the Japan Society for the Promotion of Science for Young Scientists.

Supporting Information Available: Characterization data of representative synthetic compounds and HPLC charts of **11a**, **11c**, **15e**, **16e**, **15q**, **16q**, **20a**, **20d**, **23d**, **23j**, **23o**, and **23p**. This material is available free of charge via the Internet at http://pubs.acs.org.

References

(1) Nagasawa, T.; Kikutani, H.; Kishimoto, T. Molecular cloning and structure of a pre-B-cell growth-stimulating factor. *Proc. Natl. Acad. Sci. U.S.A.* **1994**, *91*, 2305−2309.
(2) Bleul, C. C.; Farzan, M.; Choe, H.; Parolin, C.; Clark-Lewis, I.; Sodroski, J.; Springer, T. A. The lymphocyte chemoattractant SDF-1 is a ligand for LESTR/fusin and blocks HIV-1 entry. *Nature* **1996**, *382*, 829−833.
(3) Oberlin, E.; Amara, A.; Bachelerie, F.; Bessia, C.; Virelizier, J.-L.; Arenzana-Seisdedos, F.; Schwartz, O.; Heard, J.-M.; Clark-Lewis, I.; Legler, D. F.; Loetscher, M.; Baggiolini, M.; Moser, B. The CXC chemokine SDF-1 is the ligand for LESTR/fusin and prevents infection by T-cell-line-adapted HIV-1. *Nature* **1996**, *382*, 833−835.
(4) Tashiro, K.; Tada, H.; Heilker, R.; Shirozu, M.; Nakano, T.; Honjo, T. Signal sequence trap: a cloning strategy for secreted proteins and type I membrane proteins. *Science* **1993**, *261*, 600−603.
(5) Feng, Y.; Broder, C. C.; Kennedy, P. E.; Berger, E. A. HIV-1 entry co-factor: Functional cDNA cloning of a seven-transmembrane, G protein-coupled receptor. *Science* **1996**, *272*, 872−877.
(6) Müller, A.; Homey, B.; Soto, H.; Ge, N.; Catron, D.; Buchanan, M. E.; McClanahan, T.; Murphy, E.; Yuan, W.; Wagner, S. N.; Barrera, J. L.; Mohar, A.; Verastegui, E.; Zlotnik, A. Involvement of chemokine receptors in breast cancer metastasis. *Nature* **2001**, *410*, 50−56.
(7) Koshiba, T.; Hosotani, R.; Miyamoto, Y.; Ida, J.; Tsuji, S.; Nakamura, S.; Kawaguchi, M.; Kobayashi, H.; Doi, R.; Hori, T.; Fujii, N.; Imamura, M. Expression of stromal cell-derived factor 1 and CXCR4 ligand receptor system in pancreatic cancer: a possible role for tumor progression. *Clin. Cancer Res.* **2000**, *6*, 3530−3535.
(8) Mori, T.; Doi, R.; Koizumi, K.; Toyoda, E.; Tulachan, S. S.; Ito, D.; Kami, K.; Masui, T.; Fujimoto, K.; Tamamura, H.; Hiramatsu, K.; Fujii, N.; Imamura, M. CXCR4 antagonist inhibits stromal cell-derived factor 1-induced migration and invasion of human pancreatic cancer. *Mol. Cancer Ther.* **2004**, *3*, 29−37.
(9) Robledo, M. M.; Bartolome, R. A.; Longo, N.; Miguel Rodriguez-Frade, J.; Mellado, M.; Longo, I.; van Muijen, G. N. P.; Sanchez-Mateos, P.; Teixido, J. Expression of functional chemokine receptors CXCR3 and CXCR4 on human melanoma cells. *J. Biol. Chem.* **2001**, *276*, 45098−45105.
(10) Taichman, R. S.; Cooper, C.; Keller, E. T.; Pienta, K. J.; Taichman, N. S.; McCauley, L. K. Use of the stromal cell-derived factor-1/CXCR4 pathway in prostate cancer matastasis to bone. *Cancer Res.* **2002**, *62*, 1832−1837.
(11) Schrader, A. J.; Lechner, O.; Templin, M.; Dittmar, K. E. J.; Machtens, S.; Mengel, M.; Probst-Kepper, M.; Franzke, A.; Wollensak, T.; Gatzlaff, P.; Atzpodien, J.; Buer, J.; Lauber, J. CXCR4/CXCL12 expression and signalling in kidney cancer. *Br. J. Cancer* **2002**, *86*, 1250−1256.
(12) Geminder, H.; Sagi-Assif, O.; Goldberg, L.; Meshel, T.; Rechavi, G.; Witz, I. P.; Ben-Baruch, A. A possible role for CXCR4 and its ligand, the CXC chemokine stromal cell-derived factor-1, in the development of bone marrow metastases in neuroblastoma. *J. Immunol.* **2001**, *167*, 4747−4757.
(13) Bertolini, F.; Dell'Agnola, C.; Mancuso, P.; Rabascio, C.; Burlini, A.; Monestiroli, S.; Gobbi, A.; Pruneri, G.; Martinelli, G. CXCR4 neutralization, a novel therapeutic approach for non-Hodgkin's lymphoma. *Cancer Res.* **2002**, *62*, 3106−3112.
(14) Kijima, T.; Maulik, G.; Ma, P. C.; Tibaldi, E. V.; Turner, R. E.; Rollins, B.; Sattler, M.; Johnson, B. E.; Salgia, R. Regulation of cellular proliferation, cytoskeletal function, and signal transduction through CXCR4 and c-Kit in small cell lung cancer cells. *Cancer Res.* **2002**, *62*, 6304−6311.
(15) Scotton, C. J.; Wilson, J. L.; Milliken, D.; Stamp, G.; Balkwill, F. R. Epithelial cancer cell migration: a role for chemokine receptors? *Cancer Res.* **2001**, *61*, 4961−4965.
(16) Scotton, C. J.; Wilson, J. L.; Scott, K.; Stamp, G.; Wilbanks, G. D.; Fricker, S.; Bridger, G.; Balkwill, F. R. Multiple actions of the chemokine CXCL12 on epithelial tumor cells in human ovarian cancer. *Cancer Res.* **2002**, *62*, 5930−5938.
(17) Sanz-Rodriguez, F.; Hidalgo, A.; Teixido, J. Chemokine stromal cell-derived factor-1α modulates VLA-4 integrin-mediated multiple myeloma cell adhesion to CS-1/fibronectin and VCAM-1. *Blood* **2001**, *97*, 346−351.
(18) Tsukada, N.; Burger, J. A.; Zvaifler, N. J.; Kipps, T. J. Distinctive features of "nurselike" cells that differentiate in the context of chronic lymphocytic leukemia. *Blood* **2002**, *99*, 1030−1037.
(19) Juarez, J.; Bradstock, K. F.; Gottlieb, D. J.; Bendall, L. J. Effects of inhibitors of the chemokine receptor CXCR4 on acute lymphoblastic leukemia cells in vitro. *Leukemia* **2003**, *17*, 1294−1300.
(20) Rubin, J. B.; Kung, A. L.; Klein, R. S.; Chan, J. A.; Sun, Y.-P.; Schmidt, K.; Kieran, M. W.; Luster, A. D.; Segal, R. A. A small-molecule antagonist of CXCR4 inhibits intracranial growth of primary brain tumors. *Proc. Natl. Acad. Sci. U.S.A.* **2003**, *100*, 13513−13518.
(21) Nanki, T.; Hayashida, K.; El-Gabalawy, H. S.; Suson, S.; Shi, K.; Girschick, H. J.; Yavuz, S.; Lipsky, P. E. Stromal cell-derived factor-1-CXC chemokine receptor 4 interactions play a central role in CD4$^+$ T cell accumulation in rheumatoid arthritis synovium. *J. Immunol.* **2000**, *165*, 6590−6598.
(22) Tamamura, H.; Xu, Y.; Hattori, T.; Zhang, X.; Arakaki, R.; Kanbara, K.; Omagari, A.; Otaka, A.; Ibuka, T.; Yamamoto, N.; Nakashima, H.; Fujii, N. A low molecular weight inhibitor against the chemokine receptor CXCR4: a strong anti-HIV peptide T140. *Biochem. Biophys. Res. Commun.* **1998**, *253*, 877−882.
(23) Tamamura, H.; Hori, A.; Kanzaki, N.; Hiramatsu, K.; Mizumoto, M.; Nakashima, H.; Yamamoto, N.; Otaka, A.; Fujii, N. T140 analogs as CXCR4 antagonists identified as anti-metastatic agents in the treatment of breast cancer. *FEBS Lett.* **2003**, *550*, 79−83.

(24) Tamamura, H.; Fujisawa, M.; Hiramatsu, K.; Mizumoto, M.; Nakashima, H.; Yamamoto, N.; Otaka, A.; Fujii, N. Identification of a CXCR4 antagonist, a T140 analog, as an anti-rheumatoid arthritis agent. *FEBS Lett.* **2004**, *569*, 99−104.
(25) Tamamura, H.; Omagari, A.; Oishi, S.; Kanamoto, T.; Yamamoto, N.; Peiper, S. C.; Nakashima, H.; Otaka, A.; Fujii, N. Pharmacophore identification of a specific CXCR4 inhibitor, T140, leads to development of effective anti-HIV agents with very high selectivity indexes. *Bioorg. Med. Chem. Lett.* **2000**, *10*, 2633−2637.
(26) Fujii, N.; Oishi, S.; Hiramatsu, K.; Araki, T.; Ueda, S.; Tamamura, H.; Otaka, A.; Kusano, S.; Terakubo, S.; Nakashima, H.; Broach, J. A.; Trent, J. O.; Wang, Z.; Peiper, S. C. Molecular-size reduction of a potent CXCR4-chemokine antagonist using orthogonal combination of conformation- and sequence-based libraries. *Angew. Chem., Int. Ed.* **2003**, *42*, 3251−3253.
(27) Fukami, T.; Nagase, T.; Fujita, K.; Hayama, T.; Niiyama, K.; Mase, T.; Nakajima, S.; Fukuroda, T.; Saeki, T.; Nishikibe, M.; Ihara, M.; Yano, M.; Ishikawa, K. Structure−activity relationships of cyclic pentapeptide endothelin A receptor antagonists. *J. Med. Chem.* **1995**, *38*, 4309−4324.
(28) Haubner, R.; Gratias, R.; Diefenbach, B.; Goodman, S. L.; Jonczyk, A.; Kessler, H. Structural and functional aspects of RGD-containing cyclic pentapeptides as highly potent and selective integrin $\alpha V\beta 3$ antagonists. *J. Am. Chem. Soc.* **1996**, *118*, 7461−7472.
(29) Spatola, A. F.; Crozet, Y.; deWit, D.; Yanagisawa, M. Rediscovering an endothelin antagonist (BQ-123): A self-deconvoluting cyclic pentapeptide library. *J. Med. Chem.* **1996**, *39*, 3842−3846.
(30) Wermuth, J.; Goodman, S. L.; Jonczyk, A.; Kessler, H. Stereoisomerism and biological activity of the selective and superactive $\alpha V\beta 3$ integrin inhibitor cyclo(−RGDfV-) and its retro-inverso peptide. *J. Am. Chem. Soc.* **1997**, *119*, 1328−1335.
(31) Haubner, R.; Finsinger, D.; Kessler, H. Stereoisomeric peptide libraries and peptidomimetics for designing selective inhibitors of the $\alpha V\beta 3$ integrin for a new cancer therapy. *Angew. Chem., Int. Ed. Engl.* **1997**, *36*, 1374−1389.
(32) Porcelli, M.; Casu, M.; Lai, A.; Saba, G.; Pinori, M.; Cappelletti, S.; Mascagni, P. Cyclic pentapeptides of chiral sequence DLDDL as scaffold for antagonism of G-protein coupled receptors: Synthesis, activity and conformational analysis by NMR and molecular dynamics of ITF 1565 a substance P inhibitor. *Biopolymers* **1999**, *50*, 211−219.
(33) Oishi, S.; Kamano, T.; Niida, A.; Odagaki, Y.; Hamanaka, N.; Yamamoto, M.; Ajito, K.; Tamamura, H.; Otaka, A.; Fujii, N. Diastereoselective synthesis of new ψ[(*E*)-CH=CMe]- and ψ-[(*Z*)-CH=CMe]-type alkene dipeptide isosteres by organocopper reagents and application to conformationally restricted cyclic RGD peptidomimetics. *J. Org. Chem.* **2002**, *67*, 6162−6173.
(34) Nikiforovich, G. V.; Kover, K. E.; Zhang, W.-J.; Marshall, G. R. Cyclopentapeptides as flexible conformational templates. *J. Am. Chem. Soc.* **2000**, *122*, 3262−3273.
(35) Tamamura, H.; Hiramatsu, K.; Ueda, S.; Wang, Z.; Kusano, S.; Terakubo, S.; Trent, J. O.; Peiper, S. C.; Yamamoto, N.; Nakashima, H.; Otaka, A.; Fujii, N. Stereoselective synthesis of [L-Arg-L/D-3-(2-naphthyl)alanine]-type (*E*)-alkene dipeptide isosteres and its application to the synthesis and biological evaluation of pseudopeptide analogues of the CXCR4 antagonist FC131. *J. Med. Chem.* **2005**, *48*, 380−391.
(36) Abdel-Magid, A. F.; Maryanoff, C. A.; Carson, K. G. Reductive amination of aldehydes and ketones by using sodium triacetoxyborohydride. *Tetrahedron Lett.* **1990**, *31*, 5595−5598.
(37) Fukuyama, T.; Jow, C.-K.; Cheung, M. 2- and 4-Nitrobenzenesulfonamides: exceptionally versatile means for preparation of secondary amines and protection of amines. *Tetrahedron Lett.* **1995**, *36*, 6373−6374.
(38) Myers, A. G.; Gleason, J. L.; Yoon, T.; Kung, D. W. Highly practical methodology for the synthesis of D- and L-*R*-amino acids, N-protected *R*-amino acids, and *N*-methyl-*R*-amino acids. *J. Am. Chem. Soc.* **1997**, *119*, 656−673.
(39) Travins, J. M.; Etzkorn, F. A. Facile synthesis of D-amino acids from an L-serine-derived aziridine. *Tetrahedron Lett.* **1998**, *39*, 9389−9392.
(40) Biagini, S. C. G.; Gibson, S. E.; Keen, S. P. Cross-metathesis of unsaturated α-amino acid derivatives. *J. Chem. Soc., Perkin. Trans. 1* **1998**, 2485−2499.
(41) Oppolzer, W.; Lienard, P. Non-destructive cleavage of *N*-acylsultams under neutral conditions: preparation of enantiomerically pure, Fmoc-protected α-amino acids. *Helv. Chim. Acta* **1992**, *75*, 2572−2582.
(42) Douat, C.; Heitz, A.; Martinez, J.; Fehrentz, J.-A. Stereoselective synthesis of allyl- and homoallylglycines. *Tetrahedron Lett.* **2001**, *42*, 3319−3321.
(43) Scholl, M.; Ding, S.; Lee, C. W.; Grubbs, R. H. Synthesis and activity of a new generation of ruthenium-based olefin metathesis catalysts coordinated with 1,3-dimesityl-4,5-dihydroimidazol-2-ylidene ligands. *Org. Lett.* **1999**, *1*, 953−956.
(44) Tamaki, M.; Han, G.; Hruby, V. J. Practical and efficient synthesis of orthogonally protected constrained 4-guanidinoprolines. *J. Org. Chem.* **2001**, *66*, 1038−1042.
(45) Tamamura, H.; Sugioka, M.; Odagaki, Y.; Omagari, A.; Kan, Y.; Oishi, S.; Nakashima, H.; Yamamoto, N.; Peiper, S. C.; Hamanaka, N.; Otaka, A.; Fujii, N. Conformational study of a highly specific CXCR4 inhibitor, T140, disclosing the close proximity of its intrinsic pharmacophores associated with strong anti-HIV activity. *Bioorg. Med. Chem. Lett.* **2001**, *11*, 359−362 and 2409.
(46) Intramolecular hydrogen bonds were not observed in the calculated structures of these cyclic pentapeptides. Thus, these peptides do not seem to exist in a characteristic turn conformation such as a βII′γ turn as reported in several papers concerning normal cyclic pentapeptides, see Weisshoff, H.; Prasang, C.; Henklein, P.; Frommel, C.; Zschunke, A.; Mugge, C. Mimicry of βII′-turns of proteins in cyclic pentapeptides with one and without D-amino acids. *Eur. J. Biochem.* **1999**, *259*, 776−788.
(47) Murakami, T.; Nakajima, T.; Koyanagi, Y.; Tachibana, K.; Fujii, N.; Tamamura, H.; Yoshida, N.; Waki, M.; Matsumoto, A.; Yoshie, O.; Kishimoto, T.; Yamamoto, N.; Nagasawa, T. A small molecule CXCR4 inhibitor that blocks T cell line-tropic HIV-1 infection. *J. Exp. Med.* **1997**, *186*, 1389−1393.
(48) Schols, D.; Struyf, S.; Van Damme, J.; Este, J. A.; Henson, G.; De Clercq, E. Inhibition of T-tropic HIV strains by selective antagonization of the chemokine receptor CXCR4. *J. Exp. Med.* **1997**, *186*, 1383−1388.
(49) Donzella, G. A.; Schols, D.; Lin, S. W.; Este J. A.; Nagashima, K. A.; Maddon, P. J.; Allaway, G. P.; Sakmar, T. P.; Henson, G.; De Clercq, E.; Moore, J. P. AMD3100, a small molecule inhibitor of HIV-1 entry via the CXCR4 co-receptor. *Nat. Med.* **1998**, *4*, 72−77.
(50) Doranz, B. J.; Grovit-Ferbas, K.; Sharron, M. P.; Mao, S.-H.; Bidwell Goetz, M.; Daar, E. S.; Doms, R. W.; O'Brien, W. A. A small-molecule inhibitor directed against the chemokine receptor CXCR4 prevents its use as an HIV-1 coreceptor. *J. Exp. Med.* **1997**, *186*, 1395−1400.
(51) Howard, O. M. Z.; Oppenheim, J. J.; Hollingshead, M. G.; Covey, J. M.; Bigelow, J.; McCormack, J. J.; Buckheit, Jr., R. W.; Clanton, D. J.; Turpin, J. A.; Rice, W. G. Inhibition of in vitro and in vivo HIV replication by a distamycin analogue that interferes with chemokine receptor function: a candidate for chemotherapeutic and microbicidal application. *J. Med. Chem.* **1998**, *41*, 2184−2193.
(52) Fujii, N.; Nakashima, H.; Tamamura, H. The Therapeutic Potential of CXCR4 Antagonists in the Treatment of HIV. *Expert Opin. Investig. Drugs* **2003**, *12*, 185−195.
(53) Tamamura, H.; Fujii, N. Two Orthogonal Approaches to Overcome Multi-Drug Resistant HIV-1s: Development of Protease Inhibitors and Entry Inhibitors Based on CXCR4 Antagonists. *Curr. Drug Targets-Infect. Disord.* **2004**, *4*, 103−110.
(54) Navenot, J. M.; Wang , Z. X.; Trent, J. O.; Murray, J. L.; Hu, Q. X.; DeLeeuw, L.; Moore, P. S.; Chang, Y.; Peiper, S. C. Molecular anatomy of CCR5 engagement by physiologic and viral chemokines and HIV-1 envelope glycoproteins: Differences in primary structural requirements for RANTES, MIP-1α, and vMIP−II binding. *J. Mol. Biol.* **2001**, *313*, 1181−1193.
(55) Miyamoto, K.; Nakagawa, T.; Kuroda, Y. Solution structure of the cytoplasmic linker between domain III−S6 and domain IV−S1 (III−IV linker) of the rat brain sodium channel in SDS micelles. *Biopolymers* **2001**, *59*, 380−393.
(56) Ludvigsen, S.; Andersen, K. V.; Poulsen, F. M. Accurate measurements of coupling-constants from 2-dimensional nuclear-magnetic-resonance spectra of proteins and determination of ϕ-angles *J. Mol. Biol.* **1991**, *217*, 731−736.

JM050009H

Elevated Serum Levels of Stromal-Derived Factor-1α Are Associated with Increased Osteoclast Activity and Osteolytic Bone Disease in Multiple Myeloma Patients

Andrew C.W. Zannettino,[1] Amanda N. Farrugia,[1] Angela Kortesidis,[2] Jim Manavis,[3] L. Bik To,[4] Sally K. Martin,[1] Peter Diamond,[1] Hirokazu Tamamura,[5] Tsvee Lapidot,[6] Nobutaka Fujii,[5] and Stan Gronthos[2]

[1]Myeloma and Mesenchymal Research Group, Matthew Roberts Foundation Laboratory and [2]Mesenchymal Stem Cell Group, Division of Haematology, Institute of Medical and Veterinary Science, Hanson Institute, and Department of Medicine, University of Adelaide; [3]Centre for Neurological Disease, Hanson Institute; [4]Division of Haematology, Institute of Medical and Veterinary Science, Adelaide, Australia; [5]Department of Bioorganic Medicinal Chemistry, Graduate School of Pharmaceutical Sciences, Kyoto University, Kyoto, Japan; and [6]Department of Immunology, Wiezmann Institute of Science, Rehovot, Israel

Abstract

Multiple myeloma (MM) is an incurable plasma cell (PC) malignancy able to mediate massive destruction of the axial and craniofacial skeleton. The aim of this study was to investigate the role of the potent chemokine, stromal-derived factor-1α (SDF-1α) in the recruitment of osteoclast precursors to the bone marrow. Our studies show that MM PC produce significant levels of SDF-1α protein and exhibit elevated plasma levels of SDF-1α when compared with normal, age-matched subjects. The level of SDF-1α positively correlated with the presence of multiple radiological bone lesions in individuals with MM, suggesting a potential role for SDF-1α in osteoclast precursor recruitment and activation. To examine this further, peripheral blood–derived $CD14^+$ osteoclast precursors were cultured in an *in vitro* osteoclast-potentiating culture system in the presence of recombinant human SDF-1α. Although failing to stimulate an increase in $TRAP^+$, multinucleated osteoclast formation, our studies show that SDF-1α mediated a dramatic increase in both the number and the size of the resorption lacunae formed. The increased osteoclast motility and activation in response to SDF-1α was associated with an increase in the expression of a number of osteoclast activation–related genes, including *RANKL*, *RANK*, *TRAP*, *MMP-9*, *CA-II*, and *Cathepsin K*. Importantly, the small-molecule CXCR4-specific inhibitor, 4F-Benzoyl-TE14011 (T140), effectively blocked osteoclast formation stimulated by the myeloma cell line, RPMI-8226. Based on these findings, we believe that the synthesis of high levels of SDF-1α by MM PC may serve to recruit osteoclast precursors to local sites within the bone marrow and enhance their motility and bone-resorbing activity. Therefore, we propose that inhibition of the CXCR4-SDF-1α axis may provide an effective means of treatment for MM-induced osteolysis. (Cancer Res 2005; 65(5): 1700-9)

Requests for reprints: Andrew C.W. Zannettino, Myeloma and Mesenchymal Research Group, Matthew Roberts Foundation Laboratory, Division of Haematology, Institute of Medical and Veterinary Science, P.O. Box 14, Rundle Mall, Adelaide 5000, Australia. Phone: 61-8-8222-3455; Fax: 61-8-8222-3139; E-mail: andrew.zannettino@imvs.sa.gov.au.

Introduction

Osteoclast-mediated bone resorption is an essential component of bone development, growth, and remodeling. However, in a variety of pathologic conditions, including the plasma cell (PC) malignancy multiple myeloma (MM), osteoclast recruitment and activity exceed osteoblast-mediated bone formation, leading to focal bone loss throughout the axial and craniofacial skeleton. This osteolytic bone disease is responsible for the most debilitating clinical symptoms of MM, which include bone pain, pathologic fractures, spinal cord compression, hypercalcemia, renal failure, and death (1).

In MM, it is well recognized that osteoclast precursors from the peripheral blood (PB) are recruited to and amass on the endosteal surface of the bone marrow (BM), at sites of MM cell infiltration. Under the influence of a variety of BM- and PC-derived hormones, growth factors, and cytokines, the preosteoclasts differentiate into multinucleated osteoclasts capable of bone resorption. These osteoclast-activating factors include tumor necrosis factor α (TNF-α), interleukin-1β, interleukin-6, macrophage colony-stimulating factor, PTHrP (2–5), and the recently discovered TNF-ligand family member, receptor activator of nuclear factor-κB ligand (RANKL; reviewed in ref. 6). RANKL, in its membrane-associated or soluble form (7, 8), binds to a TNF receptor family member expressed by osteoclast precursors, termed RANK (9) and activates NF-κB via TNF receptor-associated factors 2, 5, and 6 (10). A soluble TNF receptor family member, termed osteoprotegerin, acts as a decoy receptor for RANKL (11). Significantly, osteoclast formation is determined principally by the ratio of RANKL to osteoprotegerin in the BM. Our recent studies (12) show that $CD38^{+++}$ human MM PC express transmembrane and soluble isoforms of RANKL mRNA and protein, respectively. Moreover, these cells lack expression of detectable osteoprotegerin, at either the protein or the transcriptional level (12). When cultured *in vitro* with PB-derived osteoclast precursors, MM cells are capable of directly supporting the formation of bone-resorbing osteoclast in a RANKL-dependent manner, as shown by inhibition studies using recombinant osteoprotegerin (12). Furthermore, our studies and those of others (13, 14) show that in most instances, transmembrane RANKL expression by MM PC correlates with the presence of osteolytic bone lesions in patients with MM.

The mechanisms by which osteoclast precursors migrate from the PB to the BM remains to be fully elucidated. Although a number of potential candidates have been suggested, recent studies by Yu et al. (15) point to a significant role for the well-characterized

chemokine, stromal derived factor-1 α (SDF-1α). SDF-1α (also termed CXCL12 or B-cell stimulating factor), was originally identified as a BM stromal and endothelial cell–derived, soluble mediator of B cell proliferation, belonging to the CXC chemokine family. Unlike other chemokines of this family, SDF-1α binds monogamously to its receptor CXCR4, which is widely expressed on leukocytes, mature dendritic cells, osteoclast precursors, and MM PC and plays key roles in cell homing to and retention in the BM (16–18). In the context of osteoclast biology, Yu et al. (15) have shown that SDF-1α increases the recruitment and migration of the murine osteoclast cell line, RAW264.7, by up-regulating the expression of the matrix degrading enzyme, matrix metalloprotease-9 (MMP-9; ref. 15). Similarly, studies by Grassi et al. (19) also show that elevated levels of SDF-1α in the synovial and bone tissue of patients with rheumatoid arthritis may promote pathologic bone loss by recruiting and activating osteoclast (19).

Although Nakayama et al. (20) recently showed that tissues enriched with plasma cells express SDF-1α mRNA, to the best of our knowledge, our study represents the first to show that purified PC and PC lines express detectable levels of SDF-1α protein. Furthermore, we show that patients with MM exhibit an elevated plasma level of MM PC–derived SDF-1α protein compared with age-matched control subjects. Importantly, this elevated level of SDF-1α is positively correlated with the presence of multiple radiological bone lesions, implicating SDF-1α in the process of osteoclast precursor recruitment and activation seen in MM.

The development of successful therapies designed to treat the skeletal destruction seen in patients with MM requires a comprehensive knowledge of the factors, which play a direct role in stimulating the migration, recruitment, and activation of osteoclasts. This study points to a potential role for SDF-1α in this process and suggests that it may provide a suitable therapeutic target for MM-mediated osteolysis. Furthermore, the measurement of serum levels of SDF-1α may ultimately enable us to predict which patients will go on to develop bone disease and may allow us to monitor the efficacy of treatment protocols directed against bone destruction.

Materials and Methods

Patients and Control Subjects. A total of 25 newly diagnosed patients, who fulfilled the diagnostic criteria for MM (21, 22), were examined in this study (Table 1). Of these, 19 exhibited X-ray-detectable osteolytic lesions. A further 12 patients, defined as monoclonal gammopathy of uncertain significance (MGUS; refs. 21, 22) and 19 normal healthy, approximately age-matched subjects were also examined. All studies were carried out with the approval of the Institutional Ethics Review Committee of the University of Adelaide, Institute of Medical and Veterinary Science and the Royal Adelaide Hospital, following written informed consent.

Cell Peripheral Blood Plasma Preparation. Human peripheral blood mononuclear cells (PBMC) were obtained from normal volunteers and isolated using Lymphoprep (Nycomed Pharma, Oslo, Norway) as previously described (23). The PBMC were washed thrice in "HHF," composed of HBSS (Life Technologies, Gaithersburg, MD), containing 5% FCS (CSL Limited, Victoria, Australia). Isolated PBMC were used as a source of osteoclast precursors as described below. Cryopreserved PBMC and BM mononuclear cell samples from MM and MGUS patients were collected by the Therapeutic Product Facility, Institute of Medical and Veterinary Science, South Australia and prepared as previously described (12).

To prepare PB plasma for SDF-1α detection, 10 mL of PB was collected into lithium/heparin–containing tubes. Samples were centrifuged for 10 minutes at 1,000 × *g* and the plasma recovered and stored at −80°C until required. To minimize loss of detectable SDF-1α, human PB plasma was prepared within 30 minutes of PB collection.

Determination of SDF-1α Levels in Normal Subjects and Patient-Derived Plasma. PB plasma SDF-1α levels were determined using a commercial SDF-1α immunoassay (Human SDF-1α, Quantikine Colorimetric Sandwich ELISA, R&D Systems, New South Wales, Australia) according to the manufacturer's recommendations. Briefly, 100 μL of "assay diluent" and 100 μL of PB plasma were added to each well and incubated for 2 hours at room temperature. The wells were washed four times with "wash buffer," after which time, 200 μL of "anti-SDF-1α conjugate" were added to each well and incubated for a further 2 hours at room temperature. The plate was washed as above, and 200 μL of "substrate solution" were added for a further 30 minutes at room temperature. The reaction was terminated by the addition of 50 μL of "stop solution," and the absorbance of each well determined using a microplate reader at 450 nm (Bio-Rad Model 3550 microplate reader, Richmond, CA). The absolute SDF-1α concentration was determined using a standard curve for SDF-1α according to the manufacturer's recommendations.

Isolation of $CD14^+$ from PBMCs. PBMCs from healthy donors were isolated as described above. CD14 positive ($CD14^+$) cells were isolated using magnetic-activated cell sorting (MACS). PBMC were incubated in blocking buffer, consisting of 10% (v/v) normal rabbit serum in HHF for 20 minutes on ice. The cells were incubated with the mouse monoclonal antibody to human CD14, FMC-17 (kindly provided by Prof. Peter McCardle, Flinders Medical Centre, Bedford Park, South Australia, Australia) for 1 hour and washed twice in HHF by centrifugation at 400 × *g*. A 1:50 dilution of goat anti-mouse γ-biotin (Southern Biotechnology Associates, Birmingham, United Kingdom) in HHF buffer was added and the cells incubated for 1 hour on ice. Cells were washed twice in MACS buffer (Ca^{2+}- and Mn^{2+}-free PBS supplemented with 1% bovine serum albumin, 5 mmol/L EDTA, and 0.01% sodium azide) as above and resuspended in a final volume of 0.9 mL MACS buffer. Streptavidin (100 μL) microbeads (Miltenyi Biotec, Bergisch Gladbach, Germany) were added to the cell suspension and incubated on ice for 15 minutes. The cell suspension was washed twice and resuspended in 0.5 mL of MACS buffer and subsequently loaded onto a mini MACS column (MS Columns, Miltenyi Biotec), and the column was washed thrice with 0.5 mL MACS buffer to retrieve the CD14 negative ($CD14^-$) cells. After addition of a further 1 mL MACS buffer, the column was removed from the magnet and the $CD14^+$ cells were isolated by positive pressure. An aliquot of cells from each fraction was stained with streptavidin-FITC and the purity assessed by flow cytometry as described below.

Osteoclast Culture Assay. Normal $CD14^+$ PBMC were isolated by MACS and plated onto 150-μm slices of elephant tusk dentine (4×10^4 cells per

Table 1. Patient and control subject information

	Number of Subjects	Mean age ± SE (range)	Female/male	Mean SDF-1α concentration ± SE (range)
MM with osteolysis	19	68.3 (44-83)	8/11	3,114.6 ± 143.3 (2,325-4,255.5)
MM without osteolysis	6	69.6 (73-81)	3/3	2,776 ± 212.9 (2,055.5-3,360)
MGUS	12	68.9 (52-84)	4/8	2,717.3 ± 110.9 (1,945.5-3,225)
Normal	19	60.26 (47-67)	9/10	2,192.8 ± 76.4 (1,499-2,950)

slice) in 96-well plates in 0.2 mL of medium consisting of α-MEM supplemented with 10% (v/v) heat inactivated (Δ) FCS, 10 nmol/L dexamethasone, 2 mmol/L L-glutamine, 20 nmol/L 1,25 $(OH)_2$ vitamin D3 (Wako Pure Chemical Industries, Osaka, Japan), and 25 ng/mL recombinant human macrophage colony-stimulating factor (Chemicon International, Temecula, CA). The $CD14^+$ monocytes were allowed to adhere overnight at 37°C in 5% CO_2 in a humidified incubator, whereupon the media was aspirated and replaced with fresh complete growth medium. The media was changed every 3 days until day 7, at which time, 50 ng/mL soluble recombinant human RANKL (rh-RANKL, Roche Applied Science, New South Wales, Australia) were added to all wells. Where indicated, 30 ng/mL recombinant human SDF-1α (rh-SDF-1α; PeproTech, Canton, MA) were added on either day 0 or day 7 and for every subsequent media change thereafter. Cultures were allowed to proceed for 14 days, after which tartrate-resistant acid phosphatase positive ($TRAP^+$), bone-resorbing osteoclast formation was assessed as described below.

In studies examining the effect of myeloma cell-derived SDF-1α, 50% (v/v) RPMI-8226 conditioned medium (CM) was added to the osteoclast precursors at day 0. RPMI-8226 cells were obtained from American Type Culture Collection (Rockville, MD) and cultured in α-MEM supplemented with 10% (v/v) ΔFCS, 2 mmol/L L-glutamine, 50 IU/mL penicillin/streptomycin (JRH, Lenexa, KS). Conditioned medium was harvested at a cell density of 1×10^6 cells/mL. To block the effects of RPMI-8226-derived and rh-SDF-1α, osteoclast precursors were incubated overnight with 5 μmol/L 4F-Benzoyl-TE14011 (T140)–truncated polyphemusin analogue, T140 (24), before the addition of fresh medium containing 50% CM or recombinant SDF-1α in combination with 5 μmol/L T140. At day 7 of culture, 50 ng/mL rh-RANKL were added to all wells to facilitate osteoclast formation and activation as described above.

In all cases, the media was changed every 3 days for the duration of the assay. Fresh T140 was added at every subsequent medium change. In contrast to the assays described above, in which osteoclast formation/activity was stimulated with rh-SDF-1α and rh-RANKL, osteoclast assays in which RPMI-8226 CM and T140 were used were allowed to proceed for a period of 21 days.

TRAP Staining of Multinucleated Osteoclast-Like Cells. Cultures on slices of dentine were fixed and stained for TRAP as recommended by the manufacturer (Sigma Chemical Co., St. Louis, MO) and as previously described (12). $TRAP^+$ cells were visualized by light microscopy and images taken with a Nikon DIH digital camera. The numbers of $TRAP^+$ cells were scored by light microscopic analysis and $TRAP^+$ cells with three or more nuclei were scored as positive. Results were enumerated in triplicate wells ± SE and the significant differences between treatments determined using Student's *t* tests (two tailed, paired), as described below.

Identification of Resorption Pit Formation. To assess bone resorption by osteoclasts following culture, dentine slices were treated with 6 mol/L ammonium hydroxide for 2 hours, ultrasonicated for 30 minutes to remove cell debris, washed in 70% ethanol, and dried overnight. The dentine slices were then mounted on stubs, carbon coated, and visualized on a Philips XL-20 scanning electron microscope, as previously described (12, 25). The number of identifiable contiguous resorption pits (resorption sites) were determined for each dentine slice. The area and/or the length of the each resorption lacunae were quantitated from scanning electron microscopic images, using SCION image analysis software (Scion Co., Frederick, MD). This software is freely available from the Scion Website (http://www.scioncorp.com) and allows the user to accurately measure the dimensions/area of resorption.

Immunohistochemical Detection of SDF-1α in Sections of BM Trephine. Five-micrometer sections of paraffin-embedded normal or MM BM trephine tissue were cut onto 3-aminopropyl-triethoxysilane–coated slides and endogenous peroxidase activity blocked by incubation with 3% H_2O_2/methanol. Microwave antigen retrieval was then done in the presence of 1 mmol/L EDTA (pH 8.0) buffer. The slides were allowed to cool to 40°C and nonspecific binding blocked by incubating sections with 3% normal horse serum for 1 hour at room temperature. The slides were then incubated overnight with either an isotype-matched, nonbinding control monoclonal antibody (1B5, IgG1) or the anti-SDF monoclonal antibody (MAB350, R&D Systems). Bound antibody was revealed using a three-step immunoperoxidase method (26) in which slides were sequentially incubated with (a) affinity-purified horseradish peroxidase–conjugated goat anti-mouse antibody (Dako, Botany, New South Wales, Australia), followed by (b) affinity-purified horseradish peroxidase–conjugated swine anti-goat immunoglobulin (Tago, Burlingame, CA), and (c) hydrogen peroxide as substrate and amino ethylcarbazole (Sigma) as the dye. Slides were counterstained briefly with hematoxylin solution and mounted in Gurr Aquamount (BDH, Poole, United Kingdom).

Reverse Transcription-PCR. Due to limiting cell numbers, gene expression studies were performed using either semiquantitative reverse transcription-PCR as previously described (12) or by real-time PCR as described below. Briefly, total RNA from cultured osteoclasts was prepared using the Trizol reagent (Life Technologies) as per manufacturer's instructions. RNA was reverse transcribed from up to 1 μg of total RNA from each sample, using a cDNA synthesis kit, as per manufacturer's recommendations (Promega Co., Madison, WI). cDNA was amplified by PCR to generate products corresponding to mRNA encoding human MMP-9, carbonic anhydrase II, cathepsin K, and TRAP using the following primer sets: human MMP-9 forward 5′-CAATCTCACCGACAGGCAGC-3′, reverse 5′-ACCGAGTTGGAACCACGAC-3′ (536-bp product); CA II forward 5′-ATGTCCCATCACTGGGGGTACG-3′, reverse 5′-GAAGTTAGTGAAGTCAGCACT-3′ (514-bp product); cathepsin K forward 5′-CTGTGGTGAGCTTTGCTCTGTA-3′, reverse 5′-TCTTCTGCACATATTGGAAGGC-3′ (546-bp product); TRAP forward 5′-CTGGCTGATGGTGCCACCCCTG-3′ and reverse 5′-CTCTCAGGCTGCAGGCTGAGG-3′ (496-bp product). The β-actin forward 5′-AGCCATGTACGTTGCTA-3′ and reverse 5′-AGTCCGCCTAGAAGCA-3′ primers were used to amplify β-actin, which was used as an internal control of RNA integrity and efficiency of the reverse transcription process. The PCR amplification products were resolved by electrophoresis on a 2% (w/v) agarose gel and visualized by SYBR Gold (Molecular Probes, Eugene, OR) staining at 570 nm. The relative amounts of PCR products were determined by quantitating the intensity of the bands using a Fluorimager and ImageQuant software (Molecular Dynamics, Sunnyvale, CA), as previously described (12). Negative controls, which had no cDNA added to the reaction mixture, were done with all PCR reactions.

Real-time PCR was employed to examine the expression of RANK, RANKL, and SDF-1α and was achieved using the IQ SYBR Green Supermix (Bio-Rad, New South Wales, Australia) on the Rotor-Gene 3000 (Corbett Research, Mortlake, New South Wales, Australia) instrument, as per manufacturers' instructions. Oligonucleotide primer sequences used were RANK forward 5′-GCTGTAACAAATGTGAACCAGGA-3′, reverse 5′-GCCTTGCCTGTATCACAAACT-3′ (154-bp product); RANKL forward 5′-TCAGCCTTTTGCTCATCTCACTAT-3′, reverse 5′-CCACCCCCGATCATGGT-3′ (96-bp product); SDF-1α forward 5′-TGCCTTCACCTCCTCTTTCA-3′, reverse 5′-AGCATGCTCTCGGAGTCG-3′ (132-bp product); and β-Actin forward 5′-GATCATTGCTCCTCCTGAGC-3′, reverse 5′-GTCATAGTCCGCCTAGAAGCAT-3′ (157-bp product). β-Actin was used as an internal control for each sample, with the relative change in mRNA levels normalized against β-actin mRNA levels. All PCRs were validated by the presence of a single peak in the melt curve analysis and amplification of a single specific product was further confirmed by electrophoresis on a 2.5% (w/v) agarose gel.

Immunofluorescence Staining of Cell Surface Antigens. Expression of CD14 and CXCR4 was determined by flow cytometry. PBMC were blocked in blocking buffer comprised of HBSS supplemented with 20 mmol/L HEPES (pH 7.35) and 5% (v/v) FCS, 2% (v/v) normal human serum, and 0.4% (v/v) bovine serum albumin, and stained with a mouse anti-CD14 (Dako, IgG1) and mouse anti-CXCR4 (Chemicon, $IgG2_b$) for 1 hour on ice. After washing twice in HHF, cells were incubated with a 1:50 dilution of goat anti-mouse $IgG2_b$-FITC and IgG1-PE antibodies (Southern Biotechnology Associates, Inc., Birmingham, AL) for 45 minutes on ice. Purified mouse isotype-matched negative control antibodies, 1B5 (IgG1) and 1A6.11 ($IgG2_b$) were a kind gift from Prof. L.K. Ashman (University of Newcastle, Australia). Following washing, all samples were analyzed on a Epics-XL-MCL flow cytometer (Beckman Coulter, Hialeah, FL) based on their forward and side light scatter properties and their FITC and PE fluorescence.

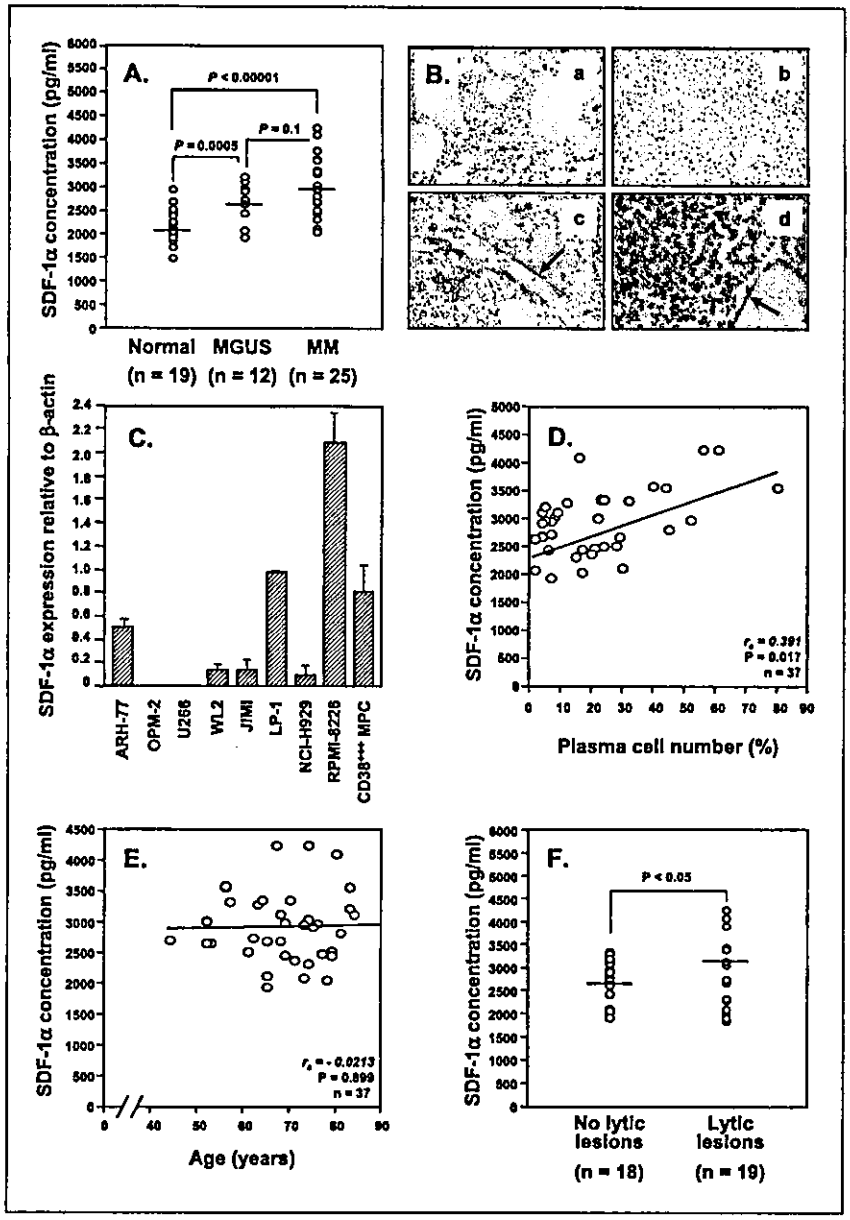

Figure 1. Myeloma plasma cells are a major source of plasma SDF-1α and elevated levels of PB plasma SDF-1α in MM patients correlates with osteolytic bone disease. *A*, level of SDF-1α in samples of peripheral blood plasma was determined using a commercial SDF-1α ELISA as described in Materials and Methods. The concentration of SDF-1α was assessed in 25 MM patients, 12 MGUS patients, and 19 normal, approximately age-matched control subjects. *B*, sections of paraffin-embedded normal (*a* and *c*) or MM BM trephine tissue (*b* and *d*) were stained with a control antibody (*a* and *b*) or an anti-SDF monoclonal antibody (*c* and *d*). All sections were counter stained with hematoxylin. In sections of normal BM tissue, large vascular structures stained positive for SDF-1α (*black arrow*, *c*), while in sections of myeloma BM tissue, essentially all identifiable myeloma plasma cells expressed appreciable levels of SDF-1α protein (*white arrow*, *d*). Original magnification ×200. *C*, real-time PCR was used to examine the expression of SDF-1α in a panel of myeloma plasma cell lines (OPM-2, U266, WL2, JIMI, LP-1, NCI-H929, and RPMI-8266), EBV transformed B cell lines (Balm and ARH-77), and purified MM patient-derived CD38^{+++} PC. Most myeloma cell lines and patient-derived PC tested expressed detectable levels of SDF-1α transcripts. *D*, correlation analysis revealed a positive correlation ($r_s = 0.391$, $P = 0.017$, $n = 37$) between plasma cell number and SDF-1α plasma levels in patients with MM. *E*, correlation analysis revealed no significant relationship ($r_s = -0.0213$, $P = 0.899$, $n = 37$) between SDF-1α plasma levels and the age of the subjects examined. *F*, MM and MGUS patients were stratified into two groups including those who exhibited no radiographic lesions ($n = 18$) and those who possessed one or more lesions in one or more sites ($n = 19$). Elevated levels of plasma SDF-1α were found to be associated with the presence of radiographically detectable osteolytic lesions ($P < 0.05$, Student's t test).

Cell Permeabilization for Immunofluorescence Staining of Intracellular Antigens. Cells were blocked in blocking buffer, washed twice in PBS, and fixed for 20 minutes in 1% paraformaldehyde at room temperature. Cells were then washed twice in HHF and 0.1% saponin (Sigma Diagnostics, Inc., St. Louis, MO) to permeabilize the membrane. Cells were immunostained as described above, with all washes and antibody dilutions in HHF and 0.1% saponin. Intracellular CXCR4 expression was detected with a mouse anti-CXCR4 monoclonal Ab (MAB170, R&D Systems).

Radiographic Identification of Skeletal Lesions. Femora, tibiae, skull, lumbar vertebrae, and pelvis were radiographed using a Faxitron X-ray system (Hewlett-Packard, McMinnville, OR), as part of routine diagnostic skeletal survey. Patients were scored as either "+" or "−" depending on the presence or absence of osteolytic lesions, respectively. Significant differences between groups were determined using the Mann-Whitney *U* test as described below.

Data Analysis. All experiments were done in triplicate, and the data is presented as mean ± SE. All statistical analysis was done using SigmaStat for Windows version 3.0 (SPSS, Inc., Chicago, IL). For parametric and nonparametric data sets, statistical analysis was done using the Mann-Whitney *U* test and the Students' *t* test, respectively. Measures of association between two variables were assessed using the Spearman Rank correlation coefficient. In all cases, $P < 0.05$ was considered significant.

Results

Elevated Levels of Plasma SDF-1α in Myeloma Patients Is Associated with the Presence of Radiographically Detectable Osteolytic Lesions. Using a commercially available ELISA kit, the level of plasma SDF-1α was determined in a cohort of individuals with MM, MGUS, and normal, approximately aged-matched controls (Table 1). As seen in Fig. 1*A*, the concentration of plasma SDF-1α was found to be significantly elevated ($P < 0.00001$, Student's *t* test) in patients with MM (3,033.4 ± 123.7) when

compared with plasma derived from normal control subjects (2,192.8 ± 76.4). Although not exhibiting a significant difference (P = 0.1, Student's t test) to patients with MM, individuals diagnosed with MGUS exhibited higher levels (P = 0.0005) of plasma SDF-1α levels (2,717.3 ± 110.9) when compared with normal controls.

To identify the source of the elevated SDF-1α in patients with MM, immunohistochemical paraffin-embedded BM trephines were examined by immunohistochemical staining. As seen in sections of normal tissue, SDF-1α expression was localized to stromal cells and the endothelial cells of large vessels [Fig. 1*B* (*c*)]. Interestingly, in sections of MM BM, SDF-1α was also expressed at high levels by myeloma PC [Fig. 1*B* (*d*)]. Consistent with this finding, real-time PCR analysis of primary human CD38^{+++} PC and a number of well characterized human MM cell lines including LP-1, RPMI-8226, WL2, JIMI, NCI-H929, and OPM-2, confirmed expression of SDF-1α by plasma cells (Fig. 1*C*).

Importantly, a positive correlation (correlation coefficient, r_s = 0.391, P = 0.017, Spearman Rank test), was observed when the plasma SDF-1α level and PC number were compared (Fig. 1*D*), suggesting that the elevated levels of SDF-1α present within plasma of MM patients was in large part, PC derived. Although in general males displayed higher levels of SDF-1α than females irrespective of disease status (2303 +/- 125 versus 2070+/- 58 for normal male

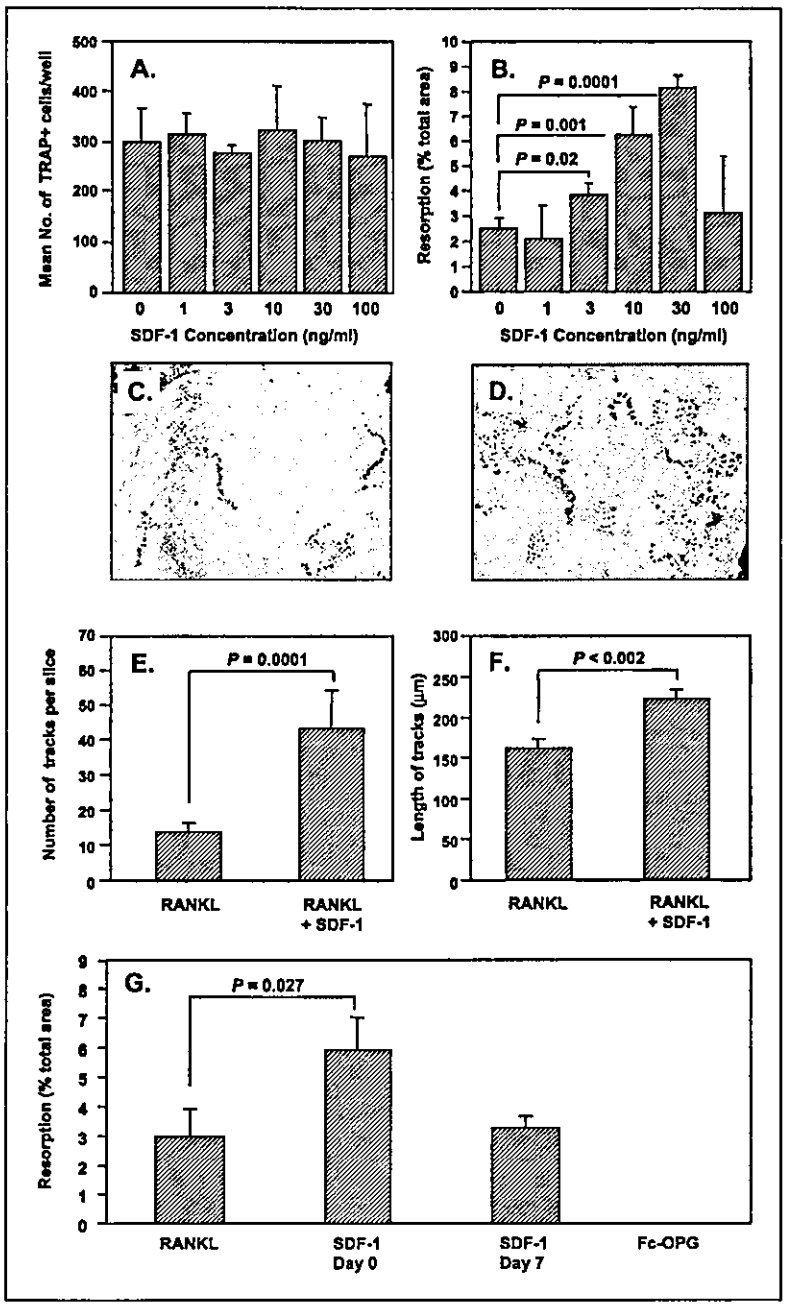

Figure 2. SDF-1α mediates enhanced bone resorption without increasing the number of TRAP$^+$ osteoclasts. CD14$^+$ MACS selected peripheral blood monocytes were cultured in the presence of rh-M-CSF (25 ng/mL) and rh-RANKL (50 ng/mL) for 14 days. SDF-1α, at 1, 3, 10, 30, and 100 ng/mL was added at day 0 or day 7 of culture. The number of TRAP$^+$ osteoclast-like cells, with three or more nuclei, was scored as positive by light microscopic analysis of stained wells after 14 days of culture. *A*, no significant differences were observed in the number of TRAP$^+$ cells generated in the presence of any of the SDF-1α concentrations used. *B*, area of the resorption, defined as regions of contiguous resorption pits, was assessed by Scion image analysis of scanning electron microscope images as described in the Materials and Methods. Area of resorption plotted as a % total area of the dentine surface per individual dentine slice ± SE for four bone slices per treatment. Notably, a significant increase in resorbed area was seen following the addition of 3 ng/mL (P = 0.02, Student's t test), 10 ng/mL (P = 0.001, Student's t test), and 30 ng/mL (P = 0.0001, Student's t test) of recombinant SDF-1α. All subsequent experiments were done with an optimal concentration of 30 ng/mL SDF-1α. Scanning electron micrographs showing the dentine resorption mediated by multinucleated TRAP$^+$ osteoclast generated following culture with RANKL alone (*C*) or RANKL with 30 ng/mL SDF-1α (*D*). Notably, although the number of TRAP$^+$ cells remained approximately the same, the area of resorbed dentine surface was greatly enhanced following the addition of 30 ng/mL SDF-1α at day 0. *Bars*, 500 μm. *E*, SDF-1α-mediated increase in bone resorption was assessed by (*E*) the number and (*F*) length of the resorption lacunae formed per individual osteoclast. The addition of SDF-1α resulted in the generation of significantly more (P = 0.0001, Student's t test) osteoclast-mediated resorption tracks. In addition, SDF-1α seemed to enhance the motility of the osteoclast, as measured by a significant (P < 0.002, Student's t test) increase in the length of the contiguous resorption lacunae (resorption track). *G*, area of resorption is plotted as % total area of the dentine surface per individual dentine slice ± SE for four bone slices per treatment. The experiments were repeated five times with three different sources of PB-derived osteoclast precursors, with similar results being obtained in all cases. Notably, no significant increase in resorbed area was seen following the addition of 30 ng/mL SDF-1α at day 7 of culture. Moreover, supplementation of media with recombinant Fc-OPG at day 7 resulted in the abolition of large TRAP$^+$ cell formation and resorption of the dentine surface, indicating that SDF-1α acts to enhance the effects of RANKL.

and females, respectively and 3382 +/- 158 versus 2684+/- 114 for MM male and females, respectively), no correlation was observed between plasma SDF-1α levels and patient age (Fig. 1*E*).

To further examine the likely *in vivo* relevance of heightened expression of SDF-1α in MM patients, we conducted a blind study to correlate SDF-1α expression with variables of bone loss in MM and MGUS patients. Radiographs of multiple bones (femora, tibiae, skull, lumbar vertebrae, and pelvis) were assessed for the presence of radiologically detectable bone lesions as part of routine diagnostic skeletal survey. Patients were subsequently stratified according to those who possessed no radiographic lesions (score = no lytic lesions, n = 18) and those who possessed one or more lesions in one or more sites (score = lytic lesions, n = 19). Correlations were then sought between osteolytic score and the level of plasma SDF-1α from the same patients as described above (Fig. 1*F*). Statistically higher levels of SDF-1α ($P < 0.05$, Student's t test) were associated with the presence of osteolytic bone lesions, suggesting that SDF-1α may have a functional role in the osteolysis observed in MM.

SDF-1α Mediates Enhanced Bone Resorption without Increasing the Number of TRAP⁺ Osteoclasts. In light of our finding that elevated SDF-1α levels correlate with osteolytic disease in MM, we next wished to examine the potential of rh-SDF-1α to stimulate the recruitment of osteoclast precursors or osteoclast function. Normal CD14⁺ human PBMC were cultured in conditions previously shown to induce osteoclastogenesis (12) in the presence or absence of a range of SDF-1α concentrations. Although not significantly influencing the number of TRAP⁺ multinucleated osteoclast formed (Fig. 2*A*), SDF-1α was found to dose-dependently stimulate an increase in osteoclastic bone resorption (Fig. 2*B*). This effect was most significant (P = 0.0001, Student's t test) when SDF-1α was used at a concentration of 30 ng/mL, and resulted in a 2- to 4-fold increase in the area of resorbed dentine substrate, when compared with cultures treated with RANKL alone (Fig. 2*D* compared with *C*). Consistent with the recent findings of Grassi et al. (19), we also found that concentrations of SDF-1α in excess of 30 ng/mL did not elicit a stimulatory effect on osteoclastic bone resorption (Fig. 2*B*).

The addition of SDF-1α at day 0 was associated with the generation of more than three times as many independent resorption lacunae per bone slice (P = 0.0001, Student's t test) when compared with untreated osteoclast (Fig. 2*E*). Furthermore, the osteoclast formed in the presence of SDF-1α were on average, 30% ($P < 0.002$, Student's t test) more motile and generated long, contiguous resorption lacunae (resorption tracks, Fig. 2*F*). As illustrated in Fig. 2*G*, both of these phenomena resulted in a significant increase (P = 0.027, Student's t test) in the area of dentine resorbed by CD14⁺ monocytes treated with both SDF-1α and RANKL (6 ± 1.2%, n = 3) as compared with cultures treated with RANKL alone (3 ± 1.1%, n = 3).

Interestingly, the addition of SDF-1α seemed to be required at an early time point during osteoclast formation, before stimulation with RANKL on day 7, as simultaneous addition of both RANKL and SDF-1α at day 7 failed to elicit any increased osteoclast activity (Fig. 2*G*). Moreover, the addition of the RANKL antagonist osteoprotegerin (Fc-osteoprotegerin) at day 7 of culture (i.e., at the time of rh-RANKL addition), abolished the formation of identifiable osteoclasts, suggesting that although SDF-1α was able to positively stimulate bone resorption, the process was still RANKL dependent. It should be noted that whereas SDF-1α was able to augment the effects of exogenous RANKL, it alone was insufficient for the generation of bone-resorbing osteoclasts (data not shown).

The SDF-1α Receptor, CXCR4, Is Down-regulated during Osteoclast Differentiation. Flow cytometry and immunohistochemical methods were used to determine if the limited temporal effectiveness of SDF-1α was related to the changes in osteoclast expression of CXCR4 following *in vitro* culture. As seen in Fig. 3*B*, our studies showed that essentially all CD14⁺ monocytes expressed high levels of the SDF-1α receptor, CXCR4 at day 0. Cultures were established in the presence or absence of SDF-1α and CXCR4 expression subsequently examined using immunohistochemical methods. CXCR4 was found to be expressed by <20% of the mononuclear cell fraction at day 7 (Fig. 3*C*), and was undetectable in multinucleated osteoclasts by day 14 of culture (Fig. 3*D*). This diminution of CXCR4, although RANKL dependent, seemed to occur independent of whether cultures were supplemented with SDF-1α (data not shown). However, omission of RANKL on day 7 of culture, resulted in little or no detectable multinucleation of the osteoclast precursors by day 14 and was associated with the retention of CXCR4 expression in ~ 10% of the cells in culture (data not shown).

SDF-1α Stimulates Resorption-Related Gene and Protein Expression. To examine the notion that SDF-1α mediated its effects by enhancing the functional activity of the osteoclast precursors and their progeny, we next did a series of experiments examining the expression of a range of osteoclast activation–related genes, using real-time PCR. We found that treatment of osteoclast precursors from day 0 with SDF-1α resulted in 7-fold increase in preosteoclast-derived expression of the RANKL at day 7

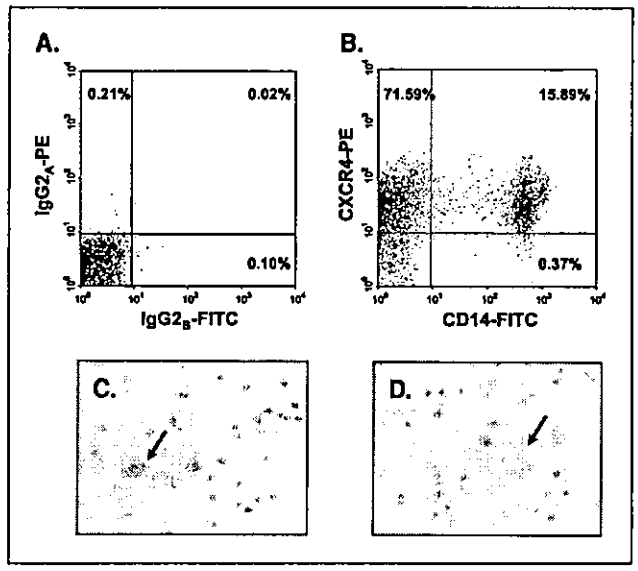

Figure 3. The SDF-1α receptor, CXCR4, is down-regulated during osteoclast differentiation. Cell-surface CXCR4 expression by peripheral blood monocytes was assessed by two-color flow cytometry. *A*, PBMC stained with isotype-matched, nonbinding control antibodies; *B*, PBMC stained with a α-CD14 monoclonal antibody and an antibody to CXCR4. Essentially all CD14 monocytes express high levels of CXCR4. The CD14-selected cells were cultured in osteoclast-inductive culture conditions as described above, and the level of CXCR4 determined using immunohistochemical methods at day 7 (*C*) and day 14 (*D*) of culture. Although most CD14⁺ monocytes expressed high levels of CXCR4 at day 0 (*B*), <20% of the preosteoclasts expressed measurable levels of CXCR4 at day 7 of culture (*black arrow*). Moreover, at day 14 of culture, CXCR4 was detectable on very few cells (<5%) and undetectable in multinucleated osteoclast-like cells.

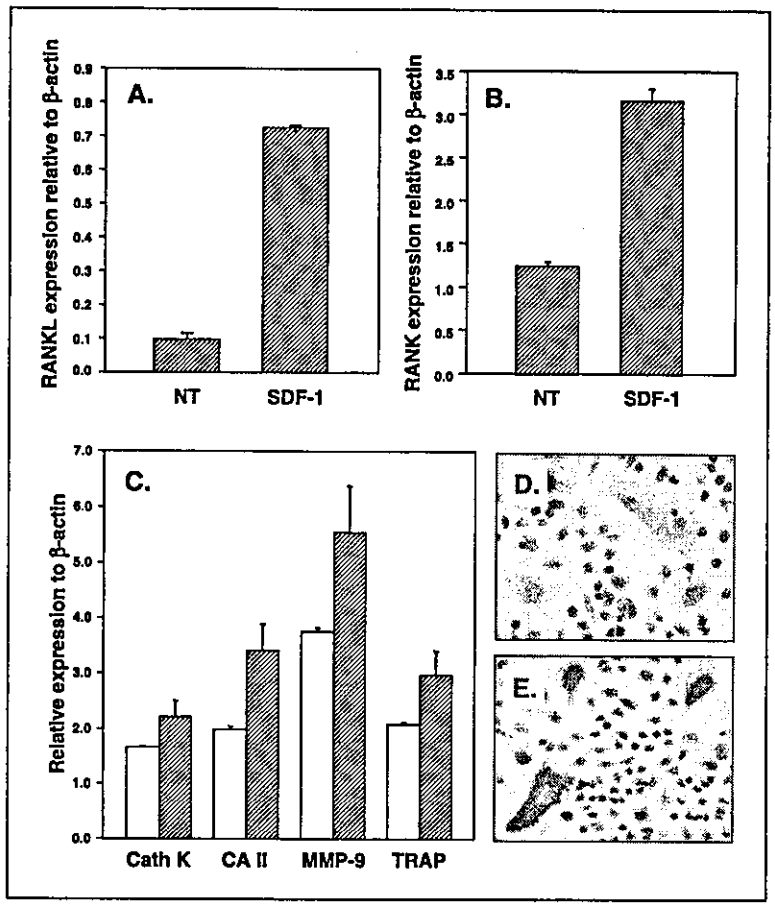

Figure 4. SDF-1α modulates the expression of osteoclast activation factors. To examine the possibility that SDF-1α mediates its effects by enhancing the functional activity of the osteoclast precursors and their progeny, a range of osteoclast activation-related genes were examined using real-time PCR. RANKL (*A*) and (*B*) RANK mRNA expression was examined in $CD14^+$ monocytes cultured in the absence (*NT*) or presence of SDF-1α at day 7 of culture. SDF-1α treatment also resulted in an elevation of RANKL and RANK expression. *C*, expression of the resorption-related markers, Cath K, CA-II, MMP-9, and TRAP were examined at day 14 by semiquantitative reverse transcription-PCR as described in Materials and Methods. In all cases, cultures grown in the presence of RANKL + SDF-1α (*shaded columns*) compared with RANKL alone (*open columns*) exhibited an elevation in the expression of all the genes examined. *D* and *E*, consistent with the gene expression analysis, cells cultured in the presence of SDF-1α stained more intensely for the resorption-related enzyme TRAP [compare RANKL (*D*) only with RANKL + SDF (*E*)].

(Fig. 4*A*). Similarly, we found that the addition of SDF-1α from day 0, was also associated with a 3-fold increase in RANK expression by the osteoclast precursors (Fig. 4*B*), suggesting that SDF-1α may serve to "prime" the preosteoclast population to the effects of rh-RANKL which was added at day 7.

Moreover, using semiquantiative reverse transcription-PCR, we also examined the effect of SDF-1α on the osteoclast expression of the resorption-related markers, MMP-9, carbonic anhydrase II, cathepsin K, and TRAP following SDF-1α treatment for 7 and 14 days. Interestingly and consistent with the findings of Yu et al. (15) and Grassi et al. (19), our studies showed that SDF-1α stimulated an up-regulation of all osteoclast-associated genes at both day 7 (data not shown) and day 14 (Fig. 4*C*). Consistent with these findings, SDF-1α treatment was associated with the generation of osteoclasts which expressed elevated levels of the TRAP enzyme in comparison with cells treated with RANKL alone (Fig. 4*D* versus *E*).

The CXCR4 Inhibitor, T140, Partially Inhibits Myeloma-Induced Osteoclastic Resorption. To show a direct "link" between myeloma cell–derived SDF-1α and the development of MM bone disease, we used the biostable, specific CXCR4 blocking agent 4F-Benzoyl-TE14011 (T140; refs. 24, 27–29) in experiments where osteoclast formation and activation was stimulated with CM from the myeloma PC line, RPMI-8226. In contrast to other MM PC lines, RPMI-8226 secrete comparatively high levels of SDF-1α (>4 ng/mL when RPMI-8226 were at a cell density of 1×10^6 cells/mL) and was therefore chosen to stimulate osteoclast formation *in vitro*. Consistent with its effects in other systems (27, 30), T140 was found to significantly inhibit both rh-SDF-1α-stimulated ($P < 0.0001$, Student's *t* test) and RPMI-8226 CM-stimulated ($P < 0.005$, Student's *t* test) osteoclast activity, as evidenced by a significant diminution of the area of resorption on the dentine slices (Fig. 5). It should be noted, that although 5 μmol/L T140 represents a relatively high concentration, we found no evidence of toxicity in control wells in which osteoclast formation was stimulated by RANKL alone.

Discussion

The α-chemokine, SDF-1α and its G protein-coupled receptor, CXCR4 regulate hematopoietic stem cell homing and anchoring in the BM and leukocyte trafficking during inflammation (16, 31–35). The critical nature of this interaction is highlighted by gene knockout studies which show that either SDF-1 or CXCR4 null mice are both lethal *in utero* due to disruptions in hematopoietic, circulatory, and nervous systems (36, 37). In addition to its role in normal physiology, other studies also implicate SDF-1/CXCR4 interactions in pathology. Various metastatic and inflammatory diseases, including the pathologic bone destruction seen in breast and prostate cancers and rheumatoid arthritis are dependent upon this critical receptor-ligand interaction (19, 38–42).

Studies from our laboratory and those of others show that primary human MM PC can directly support osteoclast development and function *in vitro*, due in large part to their synthesis of the principal osteoclastogenic factor, RANKL. This finding adds to

the growing list of myeloma PC-derived osteoclast activating factors, which include interleukin-6, interleukin-1β, TNF-α, PTHrP, and the chemokine macrophage inflammatory protein-1α. Recently, studies by Yu et al. (15, 43) suggested a role SDF-1α in normal physiologic bone remodeling by increasing osteoclast recruitment and migration to the BM. Their studies showed that the SDF-1α enhanced the migratory capacity of the osteoclast cell line, RAW264.7 by up-regulating the expression of the matrix-degrading enzyme, MMP-9 (15, 43). Whereas these studies failed to show any effect of SDF-1α on RANKL-mediated osteoclast differentiation or resorption, a more recent study by Grassi et al. (19) showed that in addition to elevating MMP-9 expression, SDF-1α also induced an increase in osteoclast activity.

We now present data showing that MM patients exhibit elevated plasma levels of SDF-1α, in comparison to normal age/sex-matched control subjects. Significantly, the plasma concentration of SDF-1α in MM patients positively correlated with the presence of osteolytic bone disease. Examination of MM BM trephines identified PC as a significant source of SDF-1α production in the BM microenvironment. These findings were confirmed using both immunohistochemical staining of PC *in situ* and by real-time PCR analysis of highly purified fluorescence-activated cell sorting–sorted $CD38^{+++}$ MM PC.

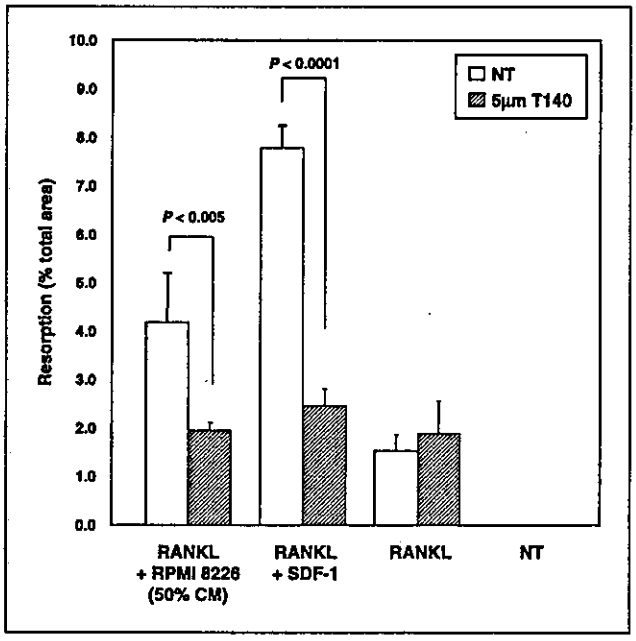

Figure 5. The CXCR4 inhibitor, T140, partially inhibits myeloma-induced osteoclastic resorption. As described in Materials and Methods, assays were established in which osteoclast formation and activation was stimulated with CM from the myeloma PC line, RPMI-8226. RPMI-8226 was selected due to its comparatively high levels of SDF-1α production (>4 ng/mL when RPMI-8226 were at a cell density of 1×10^6 cells/mL). To show a direct association between myeloma cell-derived SDF-1α and the development of MM bone disease, the polyphemusin T140 was used. At a concentration of 5 μmol/L, T140 was found to significantly inhibit both rh-SDF-1α-stimulated ($P < 0.0001$, Student's *t* test) and RPMI-8226 CM-stimulated ($P < 0.005$, Student's t test) osteoclast activity, as shown by a significant decrease in the area of resorption on the dentine slices. T140 (5 μmol/L) displayed no toxicity in control wells in which osteoclast formation was stimulated by RANKL alone. In control wells, which received no osteoclastogenic stimuli (*NT*), no detectable osteoclast-mediated resorption occurred, highlighting the importance of RANKL and/or SDF-1 in this process. The experiments were repeated thrice with different sources of PB-derived osteoclast precursors, with similar results being obtained in all cases.

In accordance with previous reports, we also found SDF-1α protein expression in BM endothelial cells comprising large blood vessels (36, 41, 44, 45). Numerous studies show that MM patients with active disease have an increased BM angiogenesis as compared with those in remission or to subjects with MGUS, a precursor of clinical MM (46, 47). In fact, increased BM microvessel density is correlated with decreased overall survival in patients with MM (48). Surprisingly, and unlike the endothelium of large vessels, the endothelium comprising the microvessels lacked measurable SDF-1α expression[7] and was therefore unlikely to be major source of the elevated plasma levels of SDF-1α. Although these studies in no way rule out the possibility that other cells in the BM may secrete SDF-1α in response to the MM PC, our data strongly support the notion that the MM PC are the major source of plasma SDF-1α, as the PC number was found to positively correlate with PB plasma SDF-1α concentration.

Considering that SDF-1α was first identified as a B-cell stimulating growth factor (36, 37, 49), and that we and others show that MM PC also express a variety of chemokine receptors, including CXCR4 (50–53), it is plausible that SDF-1α may also act as both an autocrine stimulator of MM tumor growth *in situ*, and as a mediator of MM PC migration to the BM from a secondary lymphoid organ (37, 49). Consequently, the production of excess levels of SDF-1 by MM PC may cause aberrant osteoclastogenesis in the confines of the BM microenvironment. This secondary effect of MM PC–secreted SDF-1, therefore, may represent a useful potential target for designing strategies to combat the progression of osteolytic destruction in MM patients.

To confirm the effect of SDF-1α on osteoclastogenesis directly, we cultured $CD14^+$ human PB-derived osteoclast precursors with rhSDF-1α in the presence or absence of RANKL. Consistent with the studies of Grassi et al. (19), we also found that the addition of SDF-1α to the cultures failed to stimulate an increase in the number of $TRAP^+$ multinucleated cells. Despite this, SDF-1α mediated a dramatic increase in both the number and the length of resorption lacunae formed on slices of dentine substrate, confirming that SDF-1α is a positive regulator of osteoclast function and motility. The addition of SDF-1α seemed to be required at the initiation of osteoclast culture formation, prior to stimulation with RANKL, because the addition of both SDF-1α and RANKL to $CD14^+$ PBMC cultures at day 7 failed to show any increase in osteoclast activity, when compared with RANKL alone. This could be accounted for by the rapid down-regulation of CXCR4 expression during culture, with or without the addition of SDF-1α. The lack of CXCR4 cell surface expression on differentiated osteoclasts has also previously been observed in RAW264.7 cells (15), following osteoclast induction *in vitro*, suggesting that SDF-1α/CXCR4 interactions are critical at the initial stages of osteoclast activation. Collectively, these studies indicate that MM PC contribute to local bone resorption due, in part, to their high production of SDF-1α. Our data are consistent with other reports showing that the affect of SDF-1α on osteoclast precursor cell migration and activation is mediated through the induction of various osteoclast-associated genes, including *RANK*, *RANKL*, *TRAP*, *MMP-9* (15, 19, 43, 54), *CA-II*, and *Cath K*.

Previous reports have identified several agents with the ability to selectively block SDF-1/CXCR4 interactions both *in vitro* and *in vivo* (55–59). In particular, two molecules, the bicyclam AMD-3100 and

[7] Zannettino and Gronthos, unpublished results.

the synthetic peptide polyphemusin II (T22) and its analogues were first described as specific and potent CXCR4 antagonists due to their ability to inhibit CXCR4-dependent HIV-1 entry and replication into T-cell lines. We now report, for the first time, that the novel small molecule CXCR4 inhibitor, T140 (24), is able to inhibit the osteoclast activating effects of rh-SDF-1α. Using T140, we also provide compelling data showing the importance of MM PC-derived SDF-1α in the osteoclasts activation process. These findings indicate that the CXCR4-SDF-1α axis plays a significant role in stimulating the resorptive activity of human osteoclasts. Because T140 is well tolerated *in vivo* (27, 28), we suggest that it may represent an effective inhibitor of the heightened osteoclastic bone resorption mediated by MM PC–derived SDF-1α. To this end, we are currently testing this hypothesis in an *in vivo* murine model of human myeloma.

Whereas consistent with the recent work of Nakayama et al. (20), our studies contrast those of Hideshima et al. (60). Despite being able to measure SDF-1α in BM-derived plasma, Hideshima et al. were unable to detect SDF-1α in samples of PB plasma. In addition, due to the modest effects of SDF-1α in promoting myeloma tumor growth, survival, and migration, they concluded that the CXCR4-SDF-1α axis would represent a poor target of novel therapeutics in MM disease. We believe that the findings presented in this article argue against this assertion, particularly in the context of providing a novel therapeutic target to control the osteolysis associated with this disease.

Acknowledgments

Received 5/13/2004; revised 11/30/2004; accepted 12/16/2004.

Grant support: National Health and Medical Research Council of Australia (A.C.W. Zannettinno, L.B. To, S. Gronthos, and A.N. Farrugia).

The costs of publication of this article were defrayed in part by the payment of page charges. This article must therefore be hereby marked advertisement in accordance with 18 U.S.C. Section 1734 solely to indicate this fact.

References

1. Mundy GR. Bone remodeling and its disorders. London: Martin Dunitz Ltd., 1995. p. 27–38.
2. Pfeilschifter J, Chenu C, Bird A, Mundy GR, Roodman GD. Interleukin-1 and tumor necrosis factor stimulate the formation of human osteoclast-like cells *in vitro*. J Bone Miner Res 1989;4:113–8.
3. Filella X, Blade J, Guillermo AL, et al. Cytokines (IL-6, TNF-α, IL-1α) and soluble interleukin-2 receptor as serum tumor markers in multiple myeloma. Cancer Detect Prev 1996;20:52-6.
4. Costes V, Portier M, Lu ZY, Rossi JF, Bataille R, Klein B. Interleukin-1 in multiple myeloma: producer cells and their role in the control of IL-6 production. Br J Haematol 1998;103:1152–60.
5. Hjorth-Hansen H, Seifert MF, Borset M, et al. Marked osteoblastopenia and reduced bone formation in a model of multiple myeloma bone disease in severe combined immunodeficiency mice. J Bone Miner Res 1999;14:256–63.
6. Hofbauer LC, Heufelder AE. Role of receptor activator of nuclear factor-κB ligand and osteoprotegerin in bone cell biology. J Mol Med 2001;79:243–53.
7. Quinn JM, Elliott J, Gillespie MT, Martin TJ. A combination of osteoclast differentiation factor and macrophage-colony stimulating factor is sufficient for both human and mouse osteoclast formation *in vitro*. Endocrinology 1998;139:4424–7.
8. Udagawa N, Takahashi N, Jimi E, et al. Osteoblasts/stromal cells stimulate osteoclast activation through expression of osteoclast differentiation factor/RANKL but not macrophage colony-stimulating factor: receptor activator of NF-κ B ligand. Bone 1999;25:517–23.
9. Yasuda H, Shima N, Nakagawa N, et al. A novel molecular mechanism modulating osteoclast differentiation and function. Bone 1999;25:109–13.
10. Gravallese EM, Galson DL, Goldring SR, Auron PE. The role of TNF-receptor family members and other TRAF-dependent receptors in bone resorption. Arthritis Res 2001;3:6–12.
11. Simonet WS, Lacey DL, Dunstan CR, et al. Osteoprotegerin: a novel secreted protein involved in the regulation of bone density. Cell 1997;89:309–19.
12. Farrugia AN, Atkins GJ, To LB, et al. Receptor activator of nuclear factor-κB ligand expression by human myeloma cells mediates osteoclast formation *in vitro* and correlates with bone destruction *in vivo*. Cancer Res 2003;63:5438–45.
13. Sezer O, Heider U, Jakob C, Eucker J, Possinger K. Human bone marrow myeloma cells express RANKL. J Clin Oncol 2002;20:353–4.
14. Heider U, Langelotz C, Jakob C, et al. Expression of receptor activator of nuclear factor κB ligand on bone marrow plasma cells correlates with osteolytic bone disease in patients with multiple myeloma. Clin Cancer Res 2003;9:1436–40.
15. Yu X, Huang Y, Collin-Osdoby P, Osdoby P. Stromal cell-derived factor-1 (SDF-1) recruits osteoclast precursors by inducing chemotaxis, matrix metalloproteinase-9 (MMP-9) activity, and collagen transmigration. J Bone Miner Res 2003;18:1404–18.
16. Lapidot T, Kollet O. The essential roles of the chemokine SDF-1 and its receptor CXCR4 in human stem cell homing and repopulation of transplanted immune-deficient NOD/SCID and NOD/SCID/B2m(null) mice. Leukemia 2002;16:1992–2003.
17. Coulomb-L'Hermin A, Amara A, Schiff C, et al. Stromal cell-derived factor 1 (SDF-1) and antenatal human B cell lymphopoiesis: expression of SDF-1 by mesothelial cells and biliary ductal plate epithelial cells. Proc Natl Acad Sci U S A 1999;96:8585–90.
18. Salcedo R, Oppenheim JJ. Role of chemokines in angiogenesis: CXCL12/SDF-1 and CXCR4 interaction, a key regulator of endothelial cell responses. Microcirculation 2003;10:359–70.
19. Grassi F, Cristino S, Toneguzzi S, Piacentini A, Facchini A, Lisignoli G. CXCL12 chemokine up-regulates bone resorption and MMP-9 release by human osteoclasts: CXCL12 levels are increased in synovial and bone tissue of rheumatoid arthritis patients. J Cell Physiol 2004;199:244–51.
20. Nakayama T, Hieshima K, Izawa D, Tatsumi Y, Kanamaru A, Yoshie O. Cutting edge: profile of chemokine receptor expression on human plasma cells accounts for their efficient recruitment to target tissues. J Immunol 2003;170:1136–40.
21. Durie BG, Salmon SE. A clinical staging system for multiple myeloma. Correlation of measured myeloma cell mass with presenting clinical features, response to treatment, and survival. Cancer 1975;36:842–54.
22. Durie BG. Staging and kinetics of multiple myeloma. Semin Oncol 1986;13:300–9.
23. Zannettino AC, Buhring HJ, Niutta S, Watt SM, Benton MA, Simmons PJ. The sialomucin CD164 (MGC-24v) is an adhesive glycoprotein expressed by human hematopoietic progenitors and bone marrow stromal cells that serves as a potent negative regulator of hematopoiesis. Blood 1998;92:2613–28.
24. Tamamura H, Xu Y, Hattori T, et al. A low-molecular-weight inhibitor against the chemokine receptor CXCR4: a strong anti-HIV peptide T140. Biochem Biophys Res Commun 1998;253:877–82.
25. Atkins GJ, Haynes DR, Geary SM, Loric M, Crotti TN, Findlay DM. Coordinated cytokine expression by stromal and hematopoietic cells during human osteoclast formation. Bone 2000;26:653–61.
26. Parker A, Smith MD. Immunohistochemical detection of cytokines and cell adhesion molecules in the synovial membrane. Methods Find Exp Clin Pharmacol 1999;21:311–9.
27. Tamamura . ujisawa M, Hiramatsu K, et al. Identification of a CXCR4 antagonist, a T140 analog, as an anti-rheumatoid arthritis agent. FEBS Lett 2004;569:99–104.
28. Tamamura H, Hori A, Kanzaki N, et al. T140 analogs as CXCR4 antagonists identified as anti-metastatic agents in the treatment of breast cancer. FEBS Lett 2003;550:79–83.
29. Zhang WB, Navenot JM, Haribabu B, et al. A point mutation that confers constitutive activity to CXCR4 reveals that T140 is an inverse agonist and that AMD3100 and ALX40-4C are weak partial agonists. J Biol Chem 2002;277:24515–21.
30. Libura J, Drukala J, Majka M, et al. CXCR4-SDF-1 signaling is active in rhabdomyosarcoma cells and regulates locomotion, chemotaxis, and adhesion. Blood 2002;100:2597–606.
31. Levesque JP, Hendy J, Takamatsu Y, Simmons PJ, Bendall LJ. Disruption of the CXCR4/CXCL12 chemotactic interaction during hematopoietic stem cell mobilization induced by GCSF or cyclophosphamide. J Clin Invest 2003;111:187–96.
32. Avigdor A, Goichberg P, Shivtiel S, et al. CD44 and hyaluronic acid cooperate with SDF-1 in the trafficking of human CD34+ stem/progenitor cells to bone marrow. Blood 2004;103:2981–9.
33. Baggiolini M. Chemokines and leukocyte traffic. Nature 1998;392:565–8.
34. Lapidot T, Petit I. Current understanding of stem cell mobilization: the roles of chemokines, proteolytic enzymes, adhesion molecules, cytokines, and stromal cells. Exp Hematol 2002;30:973–81.
35. Petit I, Szyper-Kravitz M, Nagler A, et al. G-CSF induces stem cell mobilization by decreasing bone marrow SDF-1 and up-regulating CXCR4. Nat Immunol 2002;3:687–94.
36. Nagasawa T, Nakajima T, Tachibana K, et al. Molecular cloning and characterization of a murine pre-B-cell growth-stimulating factor/stromal cell-derived factor 1 receptor, a murine homolog of the human immunodeficiency virus 1 entry coreceptor fusin. Proc Natl Acad Sci U S A 1996;93:14726–9.
37. Ma Q, Jones D, Borghesani PR, et al. Impaired B-lymphopoiesis, myelopoiesis, and derailed cerebellar neuron migration in CXCR4- and SDF-1-deficient mice. Proc Natl Acad Sci U S A 1998;95:9448–53.
38. Szekanecz Z, Kim J, Koch AE. Chemokines and chemokine receptors in rheumatoid arthritis. Semin Immunol 2003;15:15–21.
39. Redlich K, Hayer S, Ricci R, et al. Osteoclasts are essential for TNF-α-mediated joint destruction. J Clin Invest 2002;110:1419–27.
40. Taichman RS, Cooper C, Keller ET, et al. Use of the stromal cell-derived factor-1/CXCR4 pathway in prostate cancer metastasis to bone. Cancer Res 2002;62:1832–7.

41. Baggiolini M. Chemokines in pathology and medicine. J Intern Med 2001;250:91–104.
42. Muller A, Homey B, Soto H, et al. Involvement of chemokine receptors in breast cancer metastasis. Nature 2001;410:50–6.
43. Yu X, Huang Y, Collin-Osdoby P, et al. SDF-1 recruits osteoclast (OC) precursors via inducing MMP 9: a mechanism independent from MMP-9 induction during RANKL-mediated OC differentiation. J Bone Miner Res M244, 2002.
44. Imai K, Kobayashi M, Wang J, et al. Selective transendothelial migration of hematopoietic progenitor cells: a role in homing of progenitor cells. Blood 1999;93:149–56.
45. Ponomaryov T, Peled A, Petit I, et al. Induction of the chemokine stromal-derived factor-1 following DNA damage improves human stem cell function. J Clin Invest 2000;106:1331–9.
46. Rajkumar SV, Mesa RA, Fonseca R, et al. Bone marrow angiogenesis in 400 patients with monoclonal gammopathy of undetermined significance, multiple myeloma, and primary amyloidosis. Clin Cancer Res 2002;8:2210–6.
47. Rajkumar SV, Kyle RA. Angiogenesis in multiple myeloma. Semin Oncol 2001;28:560–4.
48. Munshi NC, Wilson C. Increased bone marrow microvessel density in newly diagnosed multiple myeloma carries a poor prognosis. Semin Oncol 2001;28:565–9.
49. Zou YR, Kottmann AH, Kuroda M, Taniuchi I, Littman DR. Function of the chemokine receptor CXCR4 in haematopolesis and in cerebellar development. Nature 1998;393:595–9.
50. Pellegrino A, Antonaci F, Russo F, et al. CXCR3-binding chemokines in multiple myeloma. Cancer Lett 2004;207:221–7.
51. Roodman GD, Choi SJ. MIP-1α and myeloma bone disease. Cancer Treat Res 2004;118:83–100.
52. Vande Broek I, Asosingh K, Vanderkerken K, Straetmans N, Van Camp B, Van Riet I. Chemokine receptor CCR2 is expressed by human multiple myeloma cells and mediates migration to bone marrow stromal cell-produced monocyte chemotactic proteins MCP-1, -2 and -3. Br J Cancer 2003;88:855–62.
53. Moller C, Stromberg T, Juremalm M, Nilsson K, Nilsson G. Expression and function of chemokine receptors in human multiple myeloma. Leukemia 2003;17:203–10.
54. Grassi F, Piacentini A, Cristino S, et al. Human osteoclasts express different CXC chemokines depending on cell culture substrate: molecular and immunocytochemical evidence of high levels of CXCL10 and CXCL12. Histochem Cell Biol 2003;120:391–400.
55. Hatse S, Princen K, Bridger G, De Clercq E, Schols D. Chemokine receptor inhibition by AMD3100 is strictly confined to CXCR4. FEBS Lett 2002;527:255–62.
56. Matthys P, Hatse S, Vermeire K, et al. AMD3100, a potent and specific antagonist of the stromal cell-derived factor-1 chemokine receptor CXCR4, inhibits autoimmune joint inflammation in IFN-γ receptor-deficient mice. J Immunol 2001;167:4686–92.
57. Hendrix CW, Flexner C, MacFarland RT, et al. Pharmacokinetics and safety of AMD-3100, a novel antagonist of the CXCR-4 chemokine receptor, in human volunteers. Antimicrob Agents Chemother 2000;44:1667–73.
58. Arakaki R, Tamamura H, Premanathan M, et al. T134, a small-molecule CXCR4 inhibitor, has no cross-drug resistance with AMD3100, a CXCR4 antagonist with a different structure. J Virol 1999;73:1719–23.
59. Murakami T, Nakajima T, Koyanagi Y, et al. A small molecule CXCR4 inhibitor that blocks T cell line-tropic HIV-1 infection. J Exp Med 1997;186:1389–93.
60. Hideshima T, Chauhan D, Hayashi T, et al. The biological sequelae of stromal cell-derived factor-1α in multiple myeloma. Mol Cancer Ther 2002;1:539–44.